3. ATMOSPHERIC MEASUREMENTS DURING PS122/5

Alexander Schulz[1], Sandro Dahlke[1], Markus Rex[1,2], Juarez Viegas[5], Matt Boyer[5,7], Zoé Brasseur[6], Ola Persson[3,4], Dietrich Althausen[15], Ola Persson[3,4], Michael Gallagher[3,4], Roberta Pirazzini[21], Byron Blomquist[3,4], Hélène Angot[3], Kevin Posman[24], Tiia Laurila[6], Andreas Preußer[20]

(not on board) Marion Maturilli[1], Matthew Shupe[3,4], Jessie Creamean[8], Heath Powers[5,9], Jim Mather[5,10], David Chu[5,9], Kerri Pratt[11], Gijs de Boer[3,4], Klaus Dethloff[1], Elizabeth Hunke[6], Wieslaw Maslowski[12], Allison McComiskey[7], David Randall[8], Michael Tjernstrom[13], David Turner[4], Johannes Verlinde[14], Ronny Engelmann[15], Hannes Griesche[15], Martin Radenz[15], Julian Hofer[15], Holger Baars[15], Patric Seifert[15], Albert Ansmann[15], Andreas Macke[15], Mario Mech[16], Bernhard Pospichal[16], Kerstin Ebell[16], Susanne Crewell[16], Gaël Dubois[17], Luc Blarel[17], Philippe Goloub[17], Andreas Raeke[18], Ian Brooks[19], Andreas Preußer[20], Ryan Neely III[19], Barbara Brooks[19], Günther Heinemann[20], Matthew Shupe[3,4], David Costa[3,4], Thomas Ayers[4], Christopher Cox[4], Christopher Fairall[4], Daniel Gottas[4], Jesse Leach[4], Sara Morris[4], Jackson Osborne[3,4], Sergio Pezoa[4], Taneil Uttal[4], Jennifer Hutchings[22], Don Perovich[23], Timothy Stanton[12], Stephen Archer[24], Detlev Helmig[3], Christopher Fairall[4], Laurens Ganzeveld[25], William Sturges[26], Dean Howard[3], Ludovic Bariteau[3,4], Hans-Werner Jacobi[27], Sjoerd Barten[25], Lucy Carpenter[28], Ivo Beck[29], Lauriane Quéléver[6], Tuija Jokinen[6], Julia Schmale[29], Mikko Sipilä[6], Tuukka Petäjä[6], Markku Kulmala[6], Thomas Ayers[2]

[1]DE.AWI
[2]DE.UNI-Potsdam
[3]EDU.CU
[4]GOV.NOAA
[5]GOV.ARM
[6]FI.UNI-Helsinki
[7]GOV.BNL
[8]EDU.CSU
[9]GOV.LANL
[10]GOV.SANDIA
[11]EDU.UMICH
[12]EDU.NPS
[13]SE.SU
[14]EDU.PSU
[15]DE.TROPOS
[16]DE.UNI-KOELN
[17]FR.UNIV-LILLE
[18]DE.DWD
[19]UK.UNI-LEEDS
[20]DE.UNITRIER
[21]FI.FMI
[22]EDU.ORSU
[23]EDU.DARTMOUTH
[24]ORG.BIGELOW
[25]NL.WUR
[26]UK.AC.UEA
[27]FR.UGA
[28]UK.AC.YORK
[29]CH.EPFL

Grant-No. AWI_PS122_00

A comprehensive summary of the atmospheric measurements during all 5 cruise legs can be found in Shupe et al., 2022.

The melt-out and abandonment of the year-long MOSAiC floe at the end of PS122/4 in the Fram Strait near the east coast of Greenland had a significant impact on the measurement activities during PS122/5. The atmospheric measurements consisted of on-board measurements during the 8-day reentry transit into the central Arctic, and on-board and on-ice measurements during the ~30 day drift of the new floe. During the 11-day exit transit at the end of MOSAiC, on-board atmospheric measurements were continued, as were some limited on-ice measurements during three ice stations as it became recognized that ample time remained. Many of the specific atmospheric measurement focii from previous MOSAiC legs were continued, though no drone measurements of the atmosphere were carried out. Leg 5 atmospheric activity had additional emphasis on interdisciplinary cross-cutting measurements

to better understand freeze-up processes during this time period, synthesis of atmospheric measurements, and measurements during the entry and exit transits. Table 3.0.1 provides an overview of the Leg 5 atmospheric activities and outlines the atmospheric chapter.

***Table 3.0.1**: List of leg 5 Team ATMOS projects*

Subchapter	Project Focus
3.1	Characterization of the atmospheric column - AWI measurements
3.2	Remote Sensing, Radiation, and Aerosols - DOE Atmospheric Radiation Management Mobile Facility
3.3	TROPOS OCEANET & Leeds Profiling – Remote sensing of clouds, aerosols & boundary layer structure
3.4	Atmospheric surface energy and momentum fluxes
3.5	Trace gas concentration and flux observations
3.6	Aerosol budget and cloud interactions
3.7	Wind and turbulence structure in the atmospheric boundary layer
3.8	Atmospheric contributions to cross-cutting efforts

The leg 5 reentry transit began with the departure of the Polarstern from the Tryoshnikov on Aug 13, 2020, near 80° 10' N, 5° W and ended when a floe was found on Aug. 21 near 87° 40' N, 105° E. The floe drifted in a generally northward direction during the next 30 days, ending at 89° 9' N, 108°E on Sep 20, at which time the Polarstern began its exit transit. The Polarstern arrived in territorial waters of Svalbard on Oct 1. Because of high-level decisions for the reentry transit track and area for floe search, the floe drift start was likely delayed by approximately 2 days and the floe drift was likely terminated 4 or 5 days earlier than necessary. The ice stations were an attempt to recover science time once the early departure was recognized.

The reentry transit due north from the NE corner of Greenland was characterized by near-freezing surface temperatures and above-freezing air between 200-2000 m altitude. The first part of the transit showed generally surface melt conditions and fog, while near the North Pole, some days with less clouds and the beginning of freezeup occurred. There was a concern that the onset of freezeup had been missed when we arrived at the new floe on Aug 21, as many melt ponds had a thin layer of ice on them. After a few days, however, surface melt restarted with the arrival of a persistent warm air mass aloft. The floe drift was characterized by episodic freeze-melt-freeze periods, with the freeze periods becoming clearly dominant in the latter half of the drift. The brief, 24-h long last melt period, however, was associated with a rain-on-snow event that had a complex atmospheric structure and produced significant changes to the snow and ice surface. The structure and consequences of this event was well captured by the second of two intensive observing periods executed during the floe drift period. Freeze-up continued throughout the exit transit, though it may have temporarily slowed during the first ice station. In general, AMSR2 showed that the ice edge advanced southward during this time.

In addition to the on-board measurements conducted by Team Atmos, we also deployed several measurement systems on the ice floe during the drift portion of the leg, and a subset of these during the exit transit ice stations. The two ASFS sleds were the first two instruments on the ice floe on Aug 21 as the camp-layout was decided. ASFS50 was placed on relatively thick ice (~130 cm) near a lead, while ASFS30 was placed at the site selected for the new Met City. The Met City tower site was an old ridge that had thick ice (> 2m), though the area was surrounded by several meltponds and bounded by a lead to the SW through NW. The infrastructure installation and instrumentation of Met city continued over the next few days, culminating in the raising of the met tower on Aug. 27. Additional atmospheric instrumentation at Met City included trace gas concentration and flux measurements at the top of the met

tower, ARM radiation sensors (Swing Set, IceRad), precipitation gauges (Precip, Parseval), and present weather detector (PWD); the FMI radiation sensors; and the ULeeds sodar. Later additions included the Naval Post-graduate School AOFB (upper ocean buoy), twol thermistor strings, and an ice mass balance buoy. ASFS30 was later moved on Sep 4 (see sections 3.4 and 3.7), as it had become redundant with the other sensors. In addition to the Met City instruments, Team Atmos (via the AWI group) deployed a fiberoptic cable capable of providing rapid temperature measurements every 60 cm from 10-m in the atmosphere to 60 m into the ocean ("Fibertown"), broadband radiometers over a nearby meltpond ("Fibertown Pond"), and a tethered balloon ("Miss Piggy"). On Sep 4, ASFS30 was moved from Met City to Hinterland and placed in a straight-line configuration with two AWI turbulence sledges, forming the "stress line" extending from a ridge area into a melt-pond studded flat ice area to the west of Met City. The new location for ASFS30 was in a meltpond, providing measurements of the heterogeneity of the freeze-up process and contributing additionally to significant cross-cutting data between the various Leg 5 MOSAiC teams. A portable trace gas concentration and flux chamber was deployed at various locations in the Central Observatory during the drift and during the exit transit ice stations. Additional surface energy budget measurements were made at 3 ice stations during the exit transit, while three ice edge crossings during the exit transit were used to obtain additional atmospheric and surface observations in this key transition zone during the beginning of the seasonal ice edge advance.

More details of these deployments and activities and a few preliminary (expected) results are described in sections 3.1 through 3.8.

References

Shupe, MD, Rex, M, Blomquist, B, Persson, POG, Schmale, J, Uttal, T, Althausen, D, Angot, H, Archer, S, Bariteau, L, Beck, I, Bilberry, J, Bucci, S, Buck, C, Boyer, M, Brasseur, Z, Brooks, IM, Calmer, R, Cassano, J, Castro, V, Chu, D, Costa, D, Cox, CJ, Creamean, J, Crewell, S, Dahlke, S, Damm, E, de Boer, G, Deckelmann, H, Dethloff, K, Dütsch, M, Ebell, K, Ehrlich, A, Ellis, J, Engelmann, R, Fong, AA, Frey, MM, Gallagher, MR, Ganzeveld, L, Gradinger, R, Graeser, J, Greenamyer, V, Griesche, H, Griffiths, S, Hamilton, J, Heinemann, G, Helmig, D, Herber, A, Heuzé, C, Hofer, J, Houchens, T, Howard, D, Inoue, J, Jacobi, H-W, Jaiser, R, Jokinen, T, Jourdan, O, Jozef, G, King, W, Kirchgaessner, A, Klingebiel, M, Krassovski, M, Krumpen, T, Lampert, A, Landing, W, Laurila, T, Lawrence, D, Lonardi, M, Loose, B, Lüpkes, C, Maahn, M, Macke, A, Maslowski, W, Marsay, C, Maturilli, M, Mech, M, Morris, S, Moser, M, Nicolaus, M, Ortega, P, Osborn, J, Pätzold, F, Perovich, DK, Petäjä, T, Pilz, C, Pirazzini, R, Posman, K, Powers, H, Pratt, KA, Preußer, A, Quéléver, L, Radenz, M, Rabe, B, Rinke, A, Sachs, T, Schulz, A, Siebert, H, Silva, T, Solomon, A, Sommerfeld, A, Spreen, G, Stephens, M, Stohl, A, Svensson, G, Uin, J, Viegas, J, Voigt, C, von der Gathen, P, Wehner, B, Welker, JM, Wendisch, M, Werner, M, Xie, ZQ, Yue, F. 2022. Overview of the MOSAiC expedition: Atmosphere. Elementa: Science of the Anthropocene 10(1). DOI: https://doi.org/10.1525/elementa.2021.00060

3.1. FROM THE SURFACE TO THE STRATOSPHERE: CHARACTERIZATION OF THE ATMOSPHERIC COLUMNZ

Alexander Schulz[1], Sandro Dahlke[1], Markus Rex[1,2]

[1]DE.AWI
[2]DE.UNI-Potsdam

(not on board) Marion Maturilli[1]

Objectives

The scientific objectives are summarized in the PS122 Expedition Programme (EXPEDITION PROGRAMME PS122 Polarstern PS122 Tromsø – Bremerhaven 20 September 2019 – 14 October 2020, available via www.awi.de/en/reports) and remained unchanged during leg 5. Routines and operational procedures developed and done during MOSAiC leg 1 to leg 3, and particularly during leg 4, had been continued. An overview of the activities and measurements

can be found in the former cruise reports. Minor adaptations of scientific priorities and technical realizations based on seasonal changes of the atmospheric physics and additional measurement platforms had been done**.** In particular during leg 5, we conducted a number of coordinated crosscutting activities – both within the ATMOS team, as well as with the ICE and OCEAN Team. These crosscutting efforts are further outlined in Section 3.7.
The special configuration during leg 5 was three-fold. First, analogous to leg 4, the complete ice camp, including our set of observational infrastructures, had to be reinstalled on the new floe. Secondly, the seasonal timing of this fifth cruise leg allowed us in a unique way to study the transition from the "summer melt" to "autumn freeze" season, which involves broad changes in surface characteristics, thermodynamics of the atmospheric column, and the near surface energy budget – all of which were specifically targeted with our observations.

Thirdly, a week-long transect of the ship along the marginal ice zone on the way back allowed unique balloon-borne observations of the vertical atmospheric column in this region, which had so far received little attention during MOSAiC.

During the leg, the ice conditions were stable in so far as that all installations remained at work and the measurements were not influenced by ice dynamics. Our operational workflow was only affected by two brief power failures from the ships electricity supply, and several occasions of freezing precipitation and icing on sensors, which implied daily maintenance work.

As an integral part of the whole MOSAiC ATMOS program, the ongoing sounding program between 12th August and 1st October continued to provide 6-hourly radiosondes and occasionally even 3- or 2-hourly ones, as is outlined below.

We started to collect data with our equipment on the ice on 25th August 2020 with a 4-component radiation sensor above a melt pond, followed by the tower measurements (DTS) on 27th August 2020, two mobile eddy covariance sledges (MECs) on 29th August 2020, and finally tethered balloon flights with the DTS sensor started on 5th September. On 29th July 2020 all instrumentation had been removed from the floe. We left the floe on 20th September 2020, and all installations were accordingly removed from the ice between 18th – 20th September. In the following, we provide a list measurement strategies and observations, that were adapted from Leg 4 (or earlier), and those that were unique during leg 5.

Operations those were adapted/continued from Leg 4:

a) Two AWI mobile eddy covariance systems (MEC sledges) were installed on the floe to sample more than one footprint area in the same time.

b) Lead experiments with both MEC systems had been not conducted. Measurements of heterogeneous footprints, especially the conduction of a form drag experiment had the highest priority due to pronounced ridge structure of the new floe. In the last half of the leg, the sledges were part of a crosscutting form drag experiment with further instruments inside team ATMOS (see Section 3.7).

c) The adapted installation of a fixed 10m tower with a fibre optic cable temperature measurement (Distributed Temperature Sensing measurement) close to Balloon Town/MetCity during leg 3 and 4 was continued and further optimized. During leg 5 we continued with the cross-cutting activity to measure the first 60m ocean temperature profile additionally to the 10m atmosphere temperature profile – so-called *Fiber Town* setup (see Cruise Report Leg 4). The setup of the leg 5 Fiber Town instrumentation was updated compared to the installation during leg 4. The fibre optic cable doesn't hang vertically 60m downward below the ice but it actively drifts by ocean currents and passively by the movement of the ice floe drift. In order to account for sub-ice drift of the fibre, we collaborated with the team OCEAN to install a pressure sensor at the end of the fibre optic cable to monitor the depths of the cable. The used sensor was RBR Duet TD 85201 (Device Operation: PS122-5_59-342, SensorWeb ID: 6785). Contact person is Mario Hoppmann (DE.AWI). As a crosscutting activity, the approach is further outlined in section 3.7 as well.

d) DTS experiments on the AWI tethered balloon platform ("Miss Piggy") had been conducted again by chance despite of harsh flight conditions, which occurred in the form of strong icing of the instruments and occasional increasing wind speed. Due to the limited number of DTS flights in earlier legs, and the fact that aerosol sampling, ozone sampling and turbulence sampling payloads had been flown extensively in earlier legs (see cruise reports from leg 1-4), the highest priority was set on DTS measurements on the modified Miss Piggy platform. As an upgrade to leg 4, we now covered and fastened the fiber cable under a tarp and net, whenever it was not used. This had to be done in order to prevent snow accumulation, icing, and floating away of the instrument in strong winds. Therefore no other instruments had been flown during leg 5 on the Miss Piggy platform.

Operations that were introduced in this Leg:

e) A radiation sensor measuring all four radiation components at 2 seconds temporal resolution was installed close to Fiber Town, facing a melt pond underneath. The aim was to observe the process of the freeze up during leg 5, when the pond, which initially had an open water surface, became progressively ice – and snow covered, thereby modulating its interaction with incoming radiation.

Work at sea

a) On-board Polarstern: Weather Balloons

During the whole leg 5 weather balloons were started from the helicopter deck on-board *Polarstern* an hour before the synoptic times 00UTC, 06UTC, 12UTC and 18UTC. This standard procedure allows that the data are transmitted near real time to the weather forecast centres via the GTS to be incorporated in the current weather forecast.

Therefore, our measurements improve the forecast of weather at our own position, as well as elsewhere in the forecast domain, and provide a valuable data point in the otherwise scarcely sampled Arctic. Additionally, we had four intense observation periods with more frequent soundings. The first one took place on September 6-7, involving the intensive observation of a strong wind event with snowfall, and contributed the following additional soundings:

Table 3.1.1: Weather balloon ascends during the first period of intensified soundings

DShip Device Operation	**Synoptic Date**
PS122/5_60-177	2020-09-06 09UTC
PS122/5_60-214	2020-09-06 15UTC
PS122/5_60-216	2020-09-06 21UTC
PS122/5_61-11	2020-09-07 03UTC
PS122/5_61-13	2020-09-07 09UTC
PS122/5_61-15	2020-09-06 15UTC

The second period of intensified soundings took place between September 12 – 15, and was to monitor the passage of another intense low pressure system, involving strong southerly winds representing a warm air intrusion, and snow/freezing rain as marked precipitation features. The additional soundings are given in the following table:

Table 3.1.2: Weather balloon ascends during the second period of intensified soundings

DShip Device Operation	**Synoptic Date**
PS122/5_61-239	2020-09-12 21UTC
PS122/5_61-240	2020-09-13 03UTC
PS122/5_61-242	2020-09-13 09UTC
PS122/5_61-250	2020-09-13 15UTC
PS122/5_61-252	2020-09-13 21UTC
PS122/5_62-6	2020-09-14 03UTC
PS122/5_62-29	2020-09-14 09UTC
PS122/5_62-31	2020-09-14 15UTC
PS122/5_62-57	2020-09-14 21UTC
PS122/5_62-54	2020-09-15 03UTC

The third period of intensified soundings occurred between September 22-23 during the transit, and was set up to measure the passage of an intense cyclone, that brought gale-force winds (the strongest winds observed during Leg 5), and inhibited a complex 3-dimensional thermodynamic structure. The associated additional soundings were:

Table 3.1.3: Weather balloon ascends during the third period of intensified soundings

DShip Device Operation	**Synoptic Date**
PS122/5_63-16	2020-09-22 15UTC
PS122/5_63-18	2020-09-22 21UTC
PS122/5_63-20	2020-09-23 03UTC
PS122/5_63-24	2020-09-23 09UTC

PS122/5_63-39	2020-09-23 15UTC
PS122/5_63-41	2020-09-23 21UTC

As we were on the transit back after the leg, the ship was passing through the marginal ice zone (MIZ) between September 24 – 30, and at occasion three half-day long ice stations enabled additional measurements on the ice. In order to capture potential particularities in the atmospheric column above the MIZ in that time, additional soundings were performed as follows:

Table 3.1.4: Weather balloon ascends during the fourth period of intensified soundings

DShip Device Operation	**Synoptic Date**
PS122/5_63-43	2020-09-24 03UTC
PS122/5_63-46	2020-09-24 09UTC
PS122/5_63-49	2020-09-24 15UTC
PS122/5_63-60	2020-09-24 21UTC
PS122/5_63-62	2020-09-25 03UTC
PS122/5_63-73	2020-09-25 21UTC
PS122/5_63-75	2020-09-26 03UTC
PS122/5_63-89	2020-09-27 08UTC
PS122/5_63-90	2020-09-27 10UTC
PS122/5_63-92	2020-09-27 14UTC
PS122/5_63-101	2020-09-27 16UTC
PS122/5_63-103	2020-09-27 20UTC
PS122/5_63-104	2020-09-27 22UTC
PS122/5_63-126	2020-09-29 15UTC
PS122/5_63-127	2020-09-29 16:30UTC
PS122/5_63-129	2020-09-29 20UTC
PS122/5_63-130	2020-09-29 22UTC
PS122/5_63-137	2020-09-30 16UTC
PS122/5_63-139	2020-09-30 20UTC
PS122/5_63-140	2020-09-30 22UTC
PS122/5_63-142	2020-10-01 02UTC
PS122/5_63-187	2020-10-01 15UTC

Standard radiosondes were further equipped with ozone add-on sensors on a regular basis (roughly weekly, 5 sondes in total, cf. Table 3.1.1). These instruments measure profiles of ozone concentration. To carry the additional payload, we use larger 1500 g balloons.

Table 3.1.5: Weather balloon ascends with ozone add-on sensors

DShip Device Operation	**Synoptic Date**
PS122/5_59-70	2020-08-17 12UTC
PS122/5_59-262	2020-08-24 18UTC
PS122/5_60-29	2020-08-31 18UTC

PS122/5_61-98	2020-09-08 18UTC
PS122/5_63-120	2020-08-31 18UTC

Between September 14 – 27, no ozone sonde was launched either because of too strong winds, significant precipitation, or because our resources were focused on taking down the camp or freight preparation.

Bathing of the balloons in oil (see leg 3) was not necessary. In total, 246 balloons were launched during leg 5. From the ordinary, 6-hourly balloons, only the one on 13th September 2020, 00UTC was missed

b) On the ice: Tethered Balloon

We equipped a Nansen sledge with all necessary tethered balloon equipment (fibre optic cable drum, tether sonde ground station, DTS System, winch, see Figure 3.1.1**)** according to our positive experience with this setup on leg 4. Miss Piggy had to be parked at about 8m height in the field. Deflation of the balloon had not been planned for wind events. However, to avoid damage to the balloon, it was put into an empty container on board *Polarstern* during 2 wind events. In total 2 different Miss Piggy setups (different DTS profiling altitudes) had been conducted which are listed below. Aiming for higher altitudes during the flights was not reasonable, because strong and / or fast icing often occurred that increased the weight of the instruments to the payload limit of the balloon.

Table 3.1.2 Measurement times on the Miss Piggy platform (based on DTS instrument time stamps)

PS122_5_60_295_XT19077_300m_MsPiggy_20200905_20200906
05.09.2020 09:52:28 UTC – 06.09.2020 04:32:27 UTC (~16.5h data, obvious invalid data removed)
PS122_5_61_328_XT19077_150m_MsPiggy_20200910_20200911
10.09.2020 10:50:14 UTC – 11.09.2020 05:55:26 UTC (~16.0h data, obvious invalid data removed)
PS122_5_61_329_XT19077_150m_MsPiggy_20200911_20200912
11.09.2020 11:24:01 UTC – 12.09.2020 11:16:27 UTC (~8.5h data, obvious invalid data removed)
PS122_5_62_283_XT19077_150m_MsPiggy_20200915_20200916
15.09.2020 09:19:39 UTC – 16.09.2020 09:05:00 UTC (~19.0h data, obvious invalid data removed)

All leg 5 flights had been configured as over night flights to sample the diurnal cycle of the atmospheric surface layer and full atmospheric boundary layer, respectively. In total about 60 measurement hours had been realized. Note however some erroneous data had been removed from the data hours estimation which had been emerged from a too strong sinking of the balloon by icing (<30m altitude). All DTS setups listed above had been configured with a temporal sampling step of 5s resulting in about 40000 temperature profiles.

We used the Silixa XT19077 DTS system and the repaired solid phase calibration bathes (SOPHABs) again (see Cruise Report Leg 4). The fibre optic cable was routed twice (after the pigtail and before the atmospheric profile) through these calibration sections to realize each section (warm and cold) two times along the fibre for each line of the helical AFL optical fibre analogous to the measurements on leg 4.

Minor issues occurred during leg 5. The tethered balloon used within the last period of leg 4 was destroyed by tipping on bamboo sticks during higher winds in the night from 6th to 7th September. During a technical test flight of tethered balloon on 4th September tether sonde F0539540 stopped to work after 30min again. We decided to use the tether sondes C1629526 and C1629505 for the next flights which also increased slightly the payload. During the night

flight from 11th to 12th September these both sondes had been damaged by tipping the ground due to icing of the tether rope and the fiber optic cable. Tether sondes C1629526 and C1629505 had been used for the last flight on 15th September 2020.

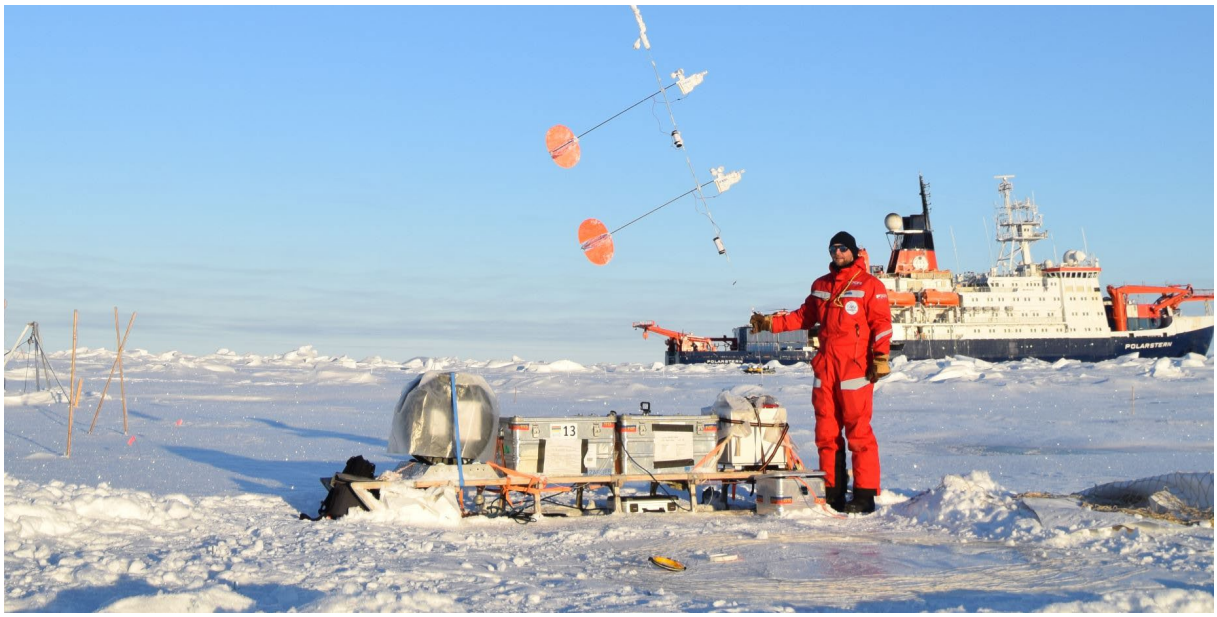

Figure 3.1.1 The measurement setup at balloon Town on September 11th . Two tether sondes are attached to the tether rope. Photo: Alexander Schulz, DE.AWI.

c) On the ice: Mobile Eddy Covariance System

The leg 5 floe could be divided in two parts. First a long ridge area parallel to the vessel and second a flat area behind this ridge. This ridge was about 100m width, several hundred meters long and less than 10m high. It had several melt ponds of different shape and characteristics embedded. One of our aims within MOSAiC was to characterize and quantify the form drag induced by increased roughness due to the ridge. Under coordination with the ATMO team (Ola Persson, EDU.CU, GOV.NOAA) we positioned both AWI MECs and the ASFS30 along a transect for an ATMO team crosscutting experiment. The MEC2 sled was positioned within the ridge, the ASFS30 on a refreezing melt pond down ridge about 130m away from MEC2 and MEC1 was positioned about 130m away from ASFS30 further down the ridge in the flat area of the floe (see floe map, Marcel Nicolaus, DE.AWI). This resulted in a roughly 260m long transect. See Figure 3.1.2 for the setup of the two AWI MECs. Within times when the wind came perpendicular to the ridge, the eddy systems collected data of the momentum fluxes along the changing surface roughness. This allows us to analyse the influence of the surface roughness on the turbulence characteristics.

For an optimal setup of this experiment, both AWI sledges had been positioned side by side close to the LOG parking area behind the ridge for an initial calibration measurement between these systems, which happened before the actual experiment.

Due to the different technical setup of the AWI MEC systems and the ASFS30 (and ASFS50) systems a final side by side calibration measurement was conducted in the remote sensing area at the end of leg 5 (after the actual experiment, contact Ola Persson EDU.CU, GOV.NOAA, Alexander Schulz, DE.AWI). The 3 resulting measurement periods of the AWI MEC systems are listed below.

Table 3.1.3 List of the mobile eddy covariance (MEC) measurements

MEC 1 LOG sledge parking area (between PPS and Target, see floe map) DShip device operation: PS122_5_59_486
29.08.2020 06:16:28 UTC – 02.09.2020 11:01:30 UTC

(~101hours, periods of sensor icing not removed)

MEC 2 LOG sledge parking area (between PPS and Target, see floe map) DShip device operation: PS122_5_59_487
29.08.2020 06:04:14 UTC – 03.09.2020 18:51:38 UTC (~132hours, periods of sensor icing not removed)

MEC 1 down ridge (about 130m away from ASFS30 @ "Hinterland", see floe map) DShip device operation: PS122_5_60_285
05.09.2020 11:22:07 UTC – 08.09.2020 02:25:05 UTC (~63hours, periods of sensor icing not removed)
09.09.2020 11:35:09 UTC – 12.09.2020 09:01:59 UTC (~69.5hours, periods of sensor icing not removed)
12.09.2020 09:06:30 UTC – 14.09.2020 04:46:05 UTC (~43.75hours, periods of sensor icing not removed)
14.09.2020 06:03:31 UTC – 18.09.2020 09:39:07 UTC (~99.5hours, periods of sensor icing not removed)

MEC 2 in ridge (about 130m away from ASFS30 @ "Hinterland" , see floe map) DShip device operation: PS122_5_60_286
05.09.2020 10:26:05 UTC – 09.09.2020 11:00:51 UTC (~96.5hours, periods of sensor icing not removed)
09.09.2020 11:09:10 UTC – 11.09.2020 18:30:33 UTC (~55.5hours, periods of sensor icing not removed)
14.09.2020 05:36:53 UTC – 18.09.2020 03:09:07 UTC (~93.5hours, periods of sensor icing not removed)

MEC 1 comparison @ remote sensing with ASFS30 and ASFS50, see floe map DShip device operation: PS122_5_62_268
19.09.2020 09:07:27 UTC – 20.09.2020 04:27:07 UTC (~19.5hours, periods of sensor icing not removed)

MEC 2 comparison @ remote sensing with ASFS30 and ASFS50, see floe map DShip device operation: PS122_5_62_269
19.09.2020 10:09:03 UTC – 20.09.2020 04:35:46 UTC (~18.5hours, periods of sensor icing not removed)

In total we collected about 396 hours of atmospheric turbulence data with each of the mobile eddy covariance systems (MEC 1 and MEC 2) during leg 5. Due to repeated icing of the sensors some data has to be excluded from the time series. Details of the measurements had been saved in field books (contact: Alexander Schulz, DE.AWI). The latest on board version of these field books had been transferred to the MCS system.

Figure 3.1.2. Left: MEC1 positioned in a flat area in down ridge direction. Right: MEC2 positioned in the ridge. Both Photographs were taken on September 9th, 2020. Photo: Alexander Schulz, DE.AWI.

d) On the ice: 10m + 60m atmosphere ocean profile tower

The 10m Fiber Town mast (see Figure 3.1.3) was installed about 50m away from the MetCity 10m mast (see floe map, Marcel Nicolaus ,DE.AWI). Apart from the additional RBR Duet TD 85201 sensor the technical setup was identical to the leg 4 for optimal continuity of the time series. First, the helical optical fibre cable (same fibre optic cable as was used on leg 4) was routed twice through the full 70m profile, resulting in 4 measurements at each point in space. Second, two solid state calibration sections (SOPHABs) had been installed to realize an optimal setup for temperature calibration in the post processing routines. We used the Silixa XT19076 system for this setup, with 10s sampling time step again.

Table 3.1.4 Measurement time of the combined 10m atmosphere and 60m ocean DTS profile

70m Fiber Town DTS temperature profile + fiber optic cable depths monitoring DShip device operation: PS122_5_59_342
27.08.2020 11:49 UTC - 18.09.2020 06:22 UTC (522.5 hours)

In total we collected about 522 hours of data resulting in about 177000 high resolution temperature profiles (time steps). Details of the measurements had been saved in field books (contact: Alexander Schulz, DE.AWI). The latest on board version of these field books had been transferred to the MCS system.

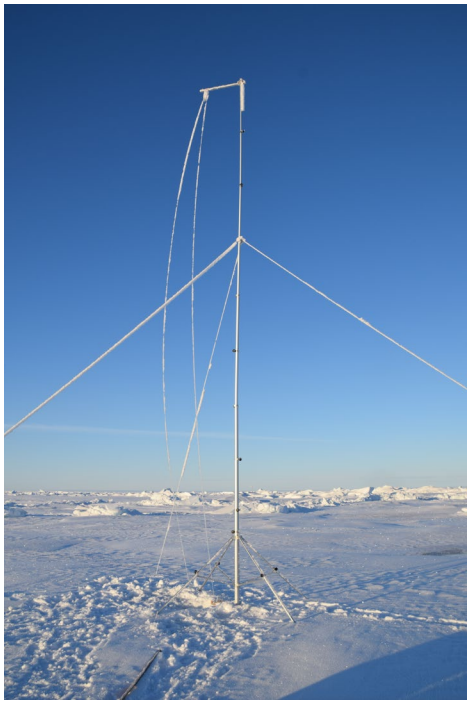

Figure 3.1.3. Fiber Town on September 11th with icing on the two fiber cables. Photo: Sandro Dahlke, DE.AWI.

e) On the ice: Monitoring of radiation components over a freezing melt pond

In coordination with Team ICE we installed our Kipp & Zonen CNR4 netradiometer on 2 pallets to monitor the Ilbedo (incoming shortwave radiation divided by outgoing short wave radiation) underneath the sensor. See Figure 3.1.4 for the setup. The heterogeneity of the ice albedo due to melt ponds is a crucial parameter and was monitored extensively by periodical albedo line measurements of the ICE team. In contrast, our instrument monitored the albedo of one specific melt pond continuously at a temporal resolution of 2 seconds. This complements the ICE team measurements within this crosscutting activity. The melt pond was located about 30m from the Fiber Town 10m mast (see floe map, Marcel Nicolaus, DE.AWI). The instrument was attached to a boom fixed on 2 pallets resulting in a measurement height of 52cm above the water/ice surface and was situated 120cm away from the pond margin. The setup was battery powered.

Table 3.1.5 Measurement time of the Kipp & Zonen CNR4 netradiometer over the melt pond

Melt pond radiation monitoring experiment DShip device operation: PS122_5_59_370
25.08.2020 10:33:24 UTC – 19.09.2020 04:26:44 UTC (estimation: 570 hours)

In total we collected about 570 hours long time series of all 4 atmospheric radiation components. One major data gap of more than 10 hours and some minor data gaps occurred due to empty batteries. All 4 domes of the sensor had been repeatedly iced and we cleaned the sensor daily. Details of the measurement had been saved in field books (contact: Alexander Schulz, DE.AWI). The latest on board version of this field books had been transferred to the MCS system.

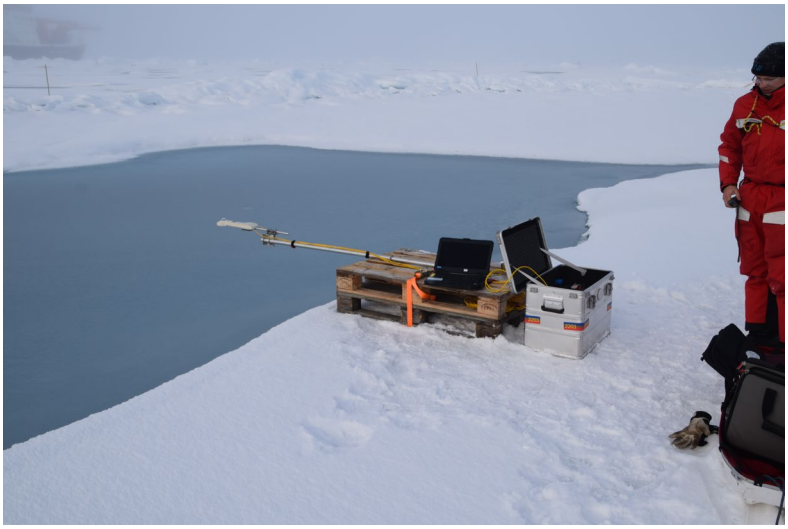

Figure 3.1.4. Pond albedo sensor upon installation on August 25th. Note the open water surface of the pond at that time. Photo: Sandro Dahlke, DE.AWI.

A fully georeferenced floe map assembled from the ALS scans (Laser scans of the floe, contact: Gerit Birnbaum, DE.AWI) with all measurement sites marked will be published in future. Personal contacts for interim floe map products are Gerit Birnbaum (DE.AWI) or Stefan Hendricks (DE.AWI) or Marcel Nicolaus (DE.AWI).

Preliminary (expected) results

Expected results from the planning phase are summarized in the PS122 Expedition Programme (EXPEDITION PROGRAMME PS122 Polarstern PS122 Tromsø – Bremerhaven 20 September 2019 – 14 October 2020, available via www.awi.de/en/reports).

a) On-board Polarstern: Weather Balloons

The comprehensive record of radiosondes gives insight into the temporal evolution of meteorological key parameters over the atmospheric column from the near surface layers up to the stratosphere, and provides a linkage to larger-scale dynamic processes in the atmosphere. Measured parameters include temperature, relative humidity, wind speed and direction. The soundings are hence expected to be useful to study the temporal evolution of synoptic features (cyclones, wind events, warm air intrusions), as well as the atmospheric features during stable, clear periods, as were observed during September 10-11. In general, the soundings provide valuable information about the larger scale synoptic state, and are expected to serve as a backbone data set to a broad variety of dedicated follow up studies involving the thermodynamics of the atmosphere.

b) On the ice: Tethered Balloon

The temporal evolution of temperature within the first hundreds meter above the ice surface complements periodical and continuous measurements in manifold way. Here we like to suppose 3 examples. First the high temporal resolution allows a detailed analysis of the temporal evolution and therefore of mixing events. Second potential disturbances of the vessel within the radio sonde profiles in the lowermost decameters can be easily identified in times when the tethered balloon measurements had been running. Third the 10m Fiber Town DTS profile was extended by a comparable measurement technique to higher altitudes. Figure 3.1.5 shows a 3 hour time height section of the flight from 5th to 6th September 2020. The vertical length along the fibre (LAF) corresponds to the temperature profile from the winch (about 80cm

above ground) to about 255m altitude. The spatio-temporal variability is striking. The horizontal lines at about 1975m LAF, and 2050m LAF correspond to artefacts resulting from the fixation of the fibre optic cable to the balloon tether. The data is the uncalibrated (preliminary), DTS-instrument (Silixa XT19077) reported temperature from only 1 of the 2 fibre strings.

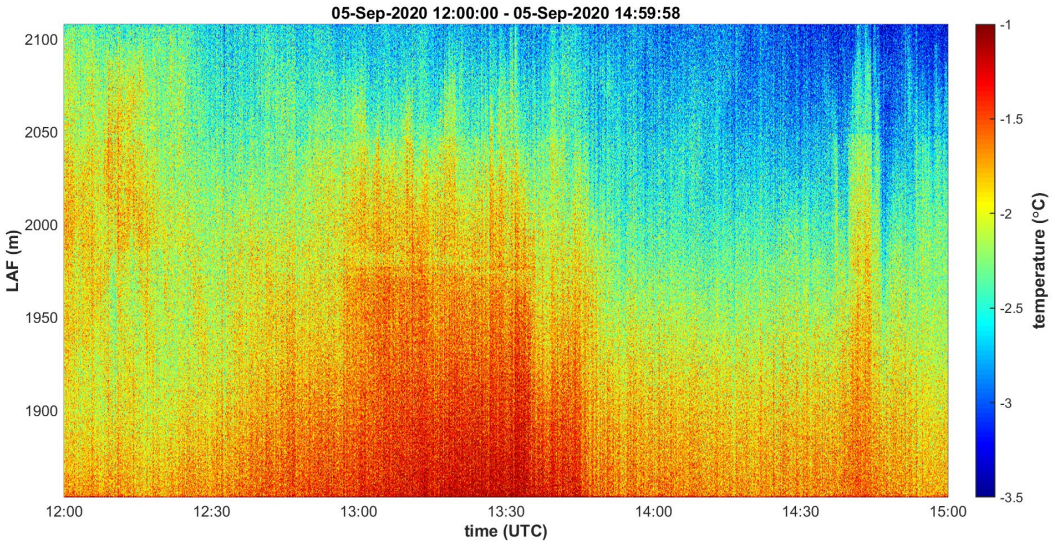

Fig. 3.1.5. 3 hour time series portion of uncalibrated (preliminary) data from the tethered balloon flight between 5th to 6th September 2020; temporal resolution 5s, spatial sampling 25cm (60cm physical resolution); vertical length along the fibre (LAF) corresponds to the temperature profile from the winch to about 255m altitude

c) On the ice: Mobile Eddy Covariance System

The leg 5 MEC measurements were completely focused on the ATMOS internal crosscutting form drag experiment. Here we expect a quantification of the changing turbulence characteristics and especially of the increased mixing due to the roughness induced turbulence. This could result in a better data basis for calculations of the drag coefficient over sea ice.

d) On the ice: 10m + 60m Atmosphere Ocean profile tower

The 70m profile realized the interconnection between the atmosphere and the ocean boundary layer with a homogenous measurement. Together with flux measurements within the atmospheres' and oceans' flux measurements (eddy covariance measurements and microstructure profiling) an optimized synthesis of the measurements concerning the intersystem exchange can be realized.

Figure 3.1.6 shows the time series of the 10m atmosphere part of the Fiber Town profile of the 14th September. The vertical length along the fibre (LAF) corresponds to the temperature profile from the ice/snow surface to about 9m altitude. In the afternoon cloud cover decreased and the temperature decreased markedly from values above the freezing point towards values of several Kelvin below freezing. The data is the uncalibrated (preliminary), DTS-instrument (Silixa XT19076) reported temperature from only 1 of the 4 fibre strings.

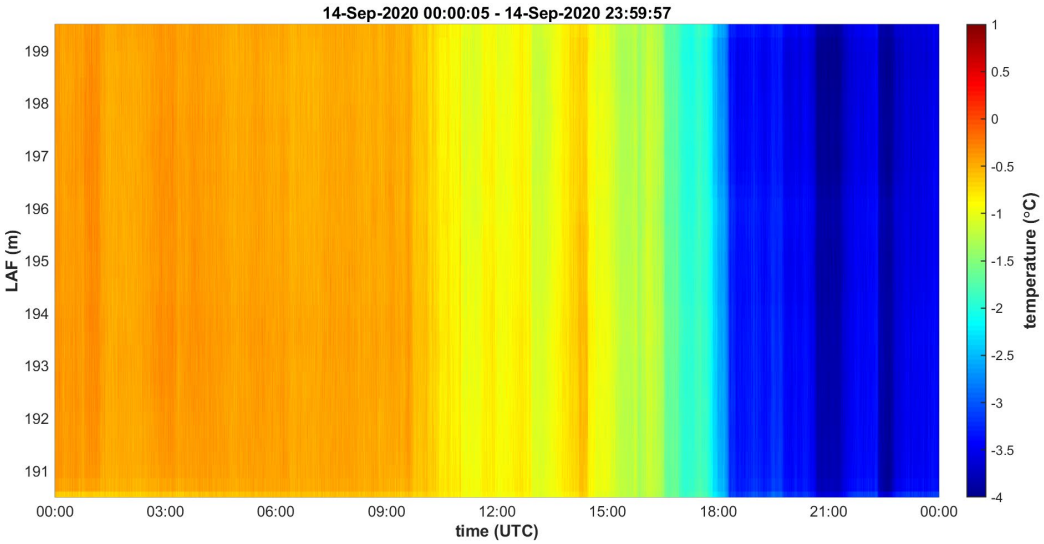

Fig. 3.1.6. time series of uncalibrated, preliminary data of the 10m atmosphere profile between 14th September 2020; temporal resolution 10s, spatial sampling 25cm (60cm physical resolution); vertical length along the fibre (LAF) corresponds to the temperature profile from the ice/snow surface to about 9m altitude

e) On the ice: Monitoring of radiation components over a freezing melt pond

Continuous measurement of the albedo over a specific melt pond allows the analysis of the temporal evolution of this crucial parameter. In leg 5 this was of particular interest, since the conditions changed from the "summer melt" season, with an open water surface on the pond, towards the "autumn freeze" season, with freezing - and snow over ice at the melt pond surface, hence providing a much brighter surface with a general increase of the albedo. Additionally to that the radiation budget over the pond is monitored allowing the synthesis with the other targeted radiation measurements (Roberta Pirazzini, **FMI**).

Data management

All data are handled, documented, archived and published following the MOSAiC data policy (see APPENDIX). All radiosonde data have been transmitted to the GTS in near real-time to assure their availability for numerical weather forecast. All sounding data (radiosonde, ozone sonde, CFH, COBALD) and according auxiliary measurements are stored in the MCS. Upon the end of leg 5, the preliminary sounding data will be processed at the GRUAN Lead Centre in Lindenberg, Germany. The final sounding data will be stored at the PANGAEA data repository (World Data Center PANGAEA Data Publisher for Earth & Environmental Science; http://www.pangaea.de/) and handled, documented, archived and published following the MOSAiC data policy.

The DTS light backscatter profiles (incl. preliminary temperature profiles) were also stored in the MCS at the end of leg 5. The final data processing of the DTS temperature profiles will be conducted at the Alfred Wegener Institute in Potsdam, Germany (contact: Alexander Schulz, alexander.schulz@awi.de, DE.AWI). Final data products will be stored at the PANGAEA data repository (World Data Center PANGAEA Data Publisher for Earth & Environmental Science; http://www.pangaea.de/) and handled, documented, archived and published following the MOSAiC data policy.

The eddy covariance data (incl. preliminary result of field processing) were stored in the MCS at the end of leg 5. The final data processing of the DTS turbulence data will be conducted at the Alfred Wegener Institute in Potsdam, Germany (contact: Alexander Schulz, alexander.schulz@awi.de, DE.AWI). Final data products will be stored at the PANGAEA data repository (World Data Center PANGAEA Data Publisher for Earth & Environmental Science;

http://www.pangaea.de/) and handled, documented, archived and published following the MOSAiC data policy.

The radiation data (incl. preliminary result of field processing) were stored in the MCS at the end of leg 5. The final data processing of the DTS turbulence data will be conducted at the Alfred Wegener Institute in Potsdam, Germany (contact: Alexander Schulz, alexander.schulz@awi.de, DE.AWI). Final data products will be stored at the PANGAEA data repository (World Data Center PANGAEA Data Publisher for Earth & Environmental Science; http://www.pangaea.de/) and handled, documented, archived and published following the MOSAiC data policy.

3.2 DOE ATMOSPHERIC RADIATION MEASUREMENT PROGRAM'S MOBILE FACILITY

Juarez Viegas[3], Matt Boyer[3,10], Zoé Brasseur[13], Ola Persson[1,2]

(not on board:) Matthew Shupe[1,2], Jessie Creamean[6], Heath Powers[3,4], Jim Mather[3,5], David Chu[3,4], Kerri Pratt[7], Gijs de Boer[1,2], Klaus Dethloff[8], Elizabeth Hunke[4], Wieslaw Maslowski[9], Allison McComiskey[10], David Randall[6], Michael Tjernstrom[11], David Turner[2], Johannes Verlinde[12]

[1]EDU.CU
[2]GOV.NOAA
[3]GOV.ARM
[4]GOV.LANL
[5]GOV.PNNL
[6]EDU.CSU
[7]EDU.UMICH
[8]DE.AWI
[9]EDU.NPS
[10]GOV.BNL
[11]SE.SU
[12]EDU.PSU
[13]FI.UNI-Helsinki

Objectives

To understand the changing Arctic sea ice at a fundamental level requires a detailed accounting of energy flow through the sea ice system. While it is clear that atmospheric energy fluxes are critically important for the sea ice energy budget, many processes controlling these fluxes, and their interactions, are poorly understood and represented in numerical models. This project aims to observe specific processes that control the flow of energy through the Arctic atmospheric system and thereby to address pressing science questions under four broad topics.

(a) Surface Energy Budget: What is the annual evolution of the surface energy budget over young sea ice? What are the key process interactions determining the surface energy budget and specifically variability in surface radiation?

(b) Clouds and Precipitation: What factors determine Arctic cloud phase partitioning? What role do clouds and precipitation play in determining low-level atmospheric structure? How does surface inhomogeneity influence the spatial structure of cloud-precipitation systems?

(c) Aerosols: How do aerosol physical, chemical, and optical properties over sea ice vary seasonally? What sources and transport patterns are responsible for variability in Arctic aerosol? What are the radiative and cloud-nucleating properties of Arctic aerosol?

(d) Boundary Layer Structure: What are the properties and effects of stably stratified turbulence in the Arctic boundary layer? What are the effects of a thinned ice cover on boundary layer

stability and heat fluxes? How do surface- and cloud-driven dynamics impact the boundary layer structure?

Work at sea

To provide the diverse and detailed atmospheric measurements needed to address the primary scientific objectives of the project, the US Department of Energy's Atmospheric Radiation Measurement (ARM) Program (www.arm.gov) has deployed its second ARM Mobile Facility (AMF-2) onboard and nearby *Polarstern* during MOSAiC. This extensive suite of instruments is operated in a collection of six laboratory sea-containers installed on the bow of *Polarstern*, one laboratory container installed on the *Polarstern* P-deck, as well as various instruments installed at Met City out on the sea ice of the Central Observatory. ARM has also provided funding support for one half of the meteorological radiosonde program led by AWI during MOSAiC, as well as personnel support for launching some of these soundings. The AMF-2 facility can be described via five instrument collections, which are captured in Table 3.2.1.

Table 3.2.1. All instruments installed and operated by the DOE ARM program, including the measurement objectives, installation location, and start date for observations.

Instrument	Measurement Objectives	Installation Location	Start of Observations
Meteorology and Winds			
Radiosonde Program (support for ½ of equipment)	Profiles of temperature and humidity	Helideck	20 Sept
Present Weather Detector (PWD)	Visibility	(1) P-deck port side; (2) Met City	17 Oct
Beam-steerable radar wind profiler (BSRWP)	Wind profiles	KAZR lab (C3)	5 Oct
Doppler lidar (DL)	Wind profiles, turbulence	Top OPS lab (C4)	7 Oct
Cloud Properties and Processes			
2-channel microwave radiometer (MWR2C)	Liquid water path and precipitable water vapor	Lower P-deck port side	16 Oct
3-channel microwave radiometer (MWR3C)	Liquid water path and precipitable water vapor	Lower P-deck port side	8 Oct
Ka-Band ARM Zenith Radar (KAZR)	Cloud occurrence and properties	KAZR lab (C3)	5 Oct
Marine W-Band ARM Cloud Radar (MWACR)	Cloud occurrence and properties	Top of OPS lab (C4)	16 Oct
High Spectral Resolution Lidar (HSRL)	Cloud & aerosol properties	OPS lab (C4)	10 Oct
Micropulse Lidar (MPL)	Cloud & aerosol properties	OPS lab (C4)	5 Oct
Ceilometer (CEIL)	Cloud base height	Lower P-deck port side	8 Oct
Total Sky Imager (TSI)	Hemispheric sky views	P-deck	23 Mar
Precipitation			

Ka-Band Scanning ARM Cloud Radar (Ka-SACR)	Cloud and precipitation spatial distribution	P-deck, starboard side	5 Oct
Parsivel2 Laser Disdrometer (LDIS)	Fall velocity and precipitation rate of precipitation	(1)P-deck port side; (2)Met City double Altar shield	(1) 30 Oct, (2) 14 Nov
Pluvio2 Weighing Bucket Rain Gauge (WBRG)	Precipitation mass	Met City in double Altar shield	30 Oct
Siphon Rain Gauge (SRG)	Precipitation mass	P-deck port side	30 Oct
Radiation			
Marine Atmospheric Emitted Radiance Interferometer (MAERI)	Spectral infrared radiation, both downwelling and upwelling	Lower P-deck port side, view to port side ice	9 Oct
Cimel Sunphotometer (CSPHOT)	Atmospheric transmission & scattering during daylight	P-deck	18 June
Fast Rotating Shadowband Radiometer (FRSR)	Direct and diffuse components of downward solar flux	P-deck	14 Oct
Ground Radiometer System (GNDRAD) – PIR, PSP	Upwelling shortwave and longwave radiation	Met City “swingset”	14 Oct
Ground Infrared Thermometer (IRT)	Ground temperature with wide field-of-view	Met City “swingset”	30 Oct
Multifilter Radiometer 3-meter (MRF3M)	Reflected radiative flux in narrow bands	Met City “swingset”	14 Oct
Ice Radiometer System (ICERAD) – PIR, PSP, SPN1	Downwelling shortwave and longwave radiation, with shortwave direct and diffuse	Met City	14 Oct
Shipboard Radiometer System (SHIPRAD) – PIR, PSP, SPN1	Downwelling shortwave and longwave radiation, with shortwave direct and diffuse	(1) P-deck port side; (2) P-deck starboard side	(1) 7 Oct; (2) 7 Oct
Sky Infrared Thermometer (IRT)	Sky temperature with narrow field-of-view	Met City “swingset”	14 Oct
Aerosols and Gases			
Automated Weather Station (AOSMET)	Pressure, temperature, relative humidity, winds	AOS inlet on AOS lab (C5)	9 Oct
Trace Gas Monitors	Concentrations: carbon monoxide, nitrous oxide, water vapor	AOS lab (C5)	9 Oct
Ozone Monitor	Concentration of ozone	AOS lab (C5)	9 Oct
Aerosol Chemical Speciation Monitor (ACSM)	Bulk chemical composition	AOS lab (C5)	8 Nov

Condensation Particle Counter (CPC)	Total particle concentration for sizes >10nm	AOS lab (C5)	8 Oct
Ultrafine Condensation Particle Counter (UCPC)	Total particle concentration for sizes >3nm	AOS lab (C5)	8 Oct
Cloud Condensation Nuclei Counter (CCN)	Concentration of cloud condensation nuclei	AOS lab (C5)	8 Nov
Scanning Mobility Particle Sizer (SMPS)	Aerosol size distribution	AOS lab (C5)	9 Oct
Ultra-High Sensitivity Aerosol Spectrometer (UHSAS)	Aerosol size distribution	AOS lab (C5)	7 Oct
Humidified Tandem Differential Mobility Analyzer (HTDMA)	Aerosol size distribution exposed to different moisture levels	AOS lab (C5)	28 Sept
Single Particle Soot Photometer (SP2)	Soot mass of aerosol particles	AOS lab (C5)	15 Oct
Particle Soot Absorption Photometer (PSAP)	Bulk aerosol absorption	AOS lab (C5)	8 Oct
Nephelometer (NEPH)	Total aerosol scattering at 450, 550, and 700 nm wavelengths	AOS lab (C5)	8 Oct

In addition to the core AMF-2 instruments, ARM has agreed via a proposal process to host and operate instrumentation for two collaborating scientists, Drs. Jessie Creamean and Kerri Pratt. These guest instruments complement the core ARM measurements by the addition of ice nucleus filters, drum samplers, and impactors, all sampling off of the Aerosol Observing System's inlet.

The ARM facility was supported on MOSAiC Leg 5 by 3 on-site technicians (Viegas, Boyer and Brasseur). Operations during Leg 5 were generally robust, with the following issues.

- The X-band Scanning ARM Cloud Radar (X-SACR) system never operated robustly in spite of many attempts to replace, fix, or modify different components; thus, the only scanning radar system available is the Ka-band component of the SACR.
- The AOS system samples air through an inlet and has a special design to minimize sampling of ship's exhaust; this includes monitoring parameters like carbon monoxide to trigger a back flow through the stack during periods of pollution. Thus, for certain periods, typically determined by wind direction, aerosol sampling was not possible.
- The 3-channel microwave radiometer (MWR3C) had a problem with the elevation motor for most of leg 3. The elevation motor failed permanently and the MWR3C was taken out of service in late April for the rest of the campaign.
- Due to software issues the Fast Rotating Shadow band Radiometer (FRSR) was not operational for the entire leg 5.
- The Single Particle Soot Photometer (SP2) was installed in the AOS on the 21st of August and was removed again on the 20th of September due to ship movement upon leaving the MOSAiC ice floe during leg 5.
- The Siphon Rain Gauge (SRG) remained out of service for the duration of Leg 5.

- The Aerosol Chemical Speciation Monitor (ACSM) continued to have periodic data outages due to power issues, but the instrument was restarted within 24 hours of any outages.
- The Micropulse Lidar (MPL) encountered a QSW fault and stopped running from the 5th of September until the end of the campaign.
- At the end of Leg 5 the TSI encountered troubles with image processing and alignment. This was most likely because of the low zenith angle of the Sun due to our position close to the North Pole.
- At the end of Leg 5, ARM instrumentation at Met City were taken down and packed away between the 17th and the 18th of September 2020.
- The HSRL showed a lot of issues during leg 5, especially during the times when the ship was moving or in transit. There are periodic outages where the laser was not lit and the computer was inaccessible.
- There were two distinct transit periods during leg 5 during which the ARM data system was partially shut down. The first transit marked the beginning of leg 5, when the Polarstern transited northwards across the North Pole to locate a new floe. The second transit occurred at the end of Leg 5, when the ship was in transit back to Bremerhaven, Germany. As a result of the data system shutdown, only a partial set of instruments will be run during the transit period. Instruments left running on the ship during the transit period continue to record data independently of the data system. During the second transit, all instruments were stopped for the rest of the campaign before arriving to Svalbard for logistical reasons.
- Other short-term issues with ARM instrumentation include temporary interruptions to operations of the MWR2C, MAERI, BSRWP, CO_N2O, MWACR, KAZR, ACSM, HSRL. Otherwise, all systems operated rather robustly for the duration of Leg 5.

Preliminary (expected) results

Primary results from the AMF-2 deployment at MOSAiC will be an extensive collection of high-quality data sets from the AMF-2 instrumentation that are as continuous as possible for the full year. These data sets will be quality assured by a large team of instrument mentors and facility managers that will not participate in the field at MOSAiC. Based on these data sets, a suite of value-added products will also be derived to provide information on geophysical parameters related to the atmospheric state, clouds, aerosols, vertical atmospheric structure, and others. These data sets are intended to support a great deal of process-based research in support of advancing knowledge, assessing models, and developing improved models for representing climate processes.

Data collected during Leg 5 will provide unique views on the clouds and precipitation associated with Arctic stratocumulus clouds and clouds linked to the 5 Arctic cyclones sampled. When combined with other MOSAiC Team Atmos data, the ARM AMF radar and wind profiling data sets are likely to provide unique understanding of dynamic forcing of precipitation in the Central Arctic, where such measurements have never or rarely before been made. The Arctic cyclone of Sep 13-14, which produced rain on snow at the surface and quickly changed the surface characteristics will certainly be studied in detail. Furthermore, utilizing the ARM AMF data set to characterize the cloud microphysics in all types of clouds during Leg 5 should enable an improved understanding of the surface radiative forcing processes during this autumn freeze-up time period, when subtle changes in surface radiation are crucial for determining if the surface ice/snow cover will melt or freeze.

Data management

All data produced by the ARM Program during MOSAiC Leg 5 has been automatically ingested and stored on ARM's onboard "site data system," which performs many operational tasks

involved with data management, initial data ingesting and formatting, data quality checks, and the production of quicklook plots of the data. Quicklooks are available via a web page to other scientists onboard *Polarstern* (https://192.168.3.33:8443) and to the general public (https://dq-amfc2.amf.arm.gov). With nearly 36 TB of data produced during Leg 5, it has been agreed that this data will not initially be uploaded to the MOSAiC Central Server, however, MOSAiC scientists can get access to the raw data through a free account on ARM's site data system (192.168.3.33:22) by obtaining credentials from the ARM data manager (see ARM technicians onsite). After MOSAiC Leg 1, and all subsequent legs, the full set of collected data are physically transported to the ARM data management facility and promptly ingested into a full set of processed data files that will then be publicly available via the ARM Data Archive (www.archive.arm.gov). Raw data will be available within a couple of weeks of its arrival at the data management facility. Based on this raw data, a suite of value-added products will also be developed in the following months, with these products also being served at the ARM Archive. Appropriate meta-data sharing and cross-linking will occur via the MOSAiC Central Storage and with PANGAEA (World Data Center PANGAEA Data Publisher for Earth & Environmental Science (www.pangaea.de)) according to the protocol agreed upon between these two archives.

References

None

3.3 REMOTE SENSING OF THE ANNUAL CYCLE OF AEROSOLS, CLOUDS, AND CORRESPONDING RADIATION CLOSURES AND BOUNDARY LAYER DYNAMICS IN THE CENTRAL ARCTIC (TROPOS – OCEANET ET AL.):

Dietrich Althausen[1]

(not on board:) Ronny Engelmann[1], Hannes Griesche[1], Martin Radenz[1], Julian Hofer[1], Holger Baars[1], Patric Seifert[1], Albert Ansmann[1], Andreas Macke[1], Mario Mech[2], Bernhard Pospichal[2], Kerstin Ebell[2], Susanne Crewell[2], Gaël Dubois[3], Luc Blarel[3], Philippe Goloub[3], Andreas Raeke[4], Ian Brooks[5], Andreas Preußer[6], Ryan Neely III[5], Barbara Brooks[5], Günther Heinemann[6]

[1]DE.TROPOS
[2]DE.UNI-KOELN
[3]FR.UNI-LILLE
[4]DE.DWD
[5]UK.UNI-LEEDS
[6]DE.UNITRIER

Objectives

Measurements of the atmospheric state in the Arctic are extremely rare and of great interest for climate research in this unique and changing environment. The mobile facility OCEANET is an ongoing observational initiative of TROPOS for aerosol and cloud profiling as well as radiation budget measurements in maritime environments onboard research vessels since 2007 (Kanitz et al., 2013, Bohlmann et al., 2018). One of the key focusses for TROPOS lies on heterogeneous ice formation processes in different areas of the world (e.g., Kanitz et al, 2011) and their radiative impact. During MOSAiC PS122/5 the OCEANET state-of-the-art en-route measurements were implemented on *Polarstern* in order to establish a full Arctic annual aerosol, cloud, and radiation data record. Also, three wind lidars were used to improve the understanding of the physical processes governing atmospheric boundary layer structure, turbulent mixing, and the interactions with both the surface and clouds in the Arctic.

The following research questions are addressed within this project:

- How do aerosol- and cloud properties influence the annual cycle of short-wave and long-wave radiation under different meteorological conditions in the Arctic?
- How often does ice formation in warm (T > –10 °C) stratus clouds occur and what are possible freezing mechanisms under clean Arctic conditions?
- Can we observe different ice-formation rates in the presence of local and long-range transported ice nucleating particles?
- Will Arctic clouds increase or suppress the currently observed Arctic warming?

An additional focus is on ESA's Aeolus wind mission. OCEANET data will also support the CAL/VAL activities of this lidar satellite within the EVAA project.

Work at sea

The OCEANET container of TROPOS was installed on the bow of *Polarstern* at the container location C8 during MOSAiC Leg 1 (see Fig. 1).

Since then, continuous measurements with the

- the multi-wavelength Raman depolarization lidar Polly^{XT} (Engelmann et al., 2016),
- the microwave radiometers HATPRO (TROPOS) and LHUMPRO (UCologne),
- the ULille CIMEL sun/sky/lunar photometer (Yin et al., 2019),
- two disdrometers: 2DVD and OTT Parsivel-2 at the bow crane,
- a total-sky imager,

- a pyranometer and a pyrgeometer at the bow crane,
- a basic DWD weather station (T,p,r.h., global radiation, long wave downward radiation)

were performed. As during Leg 4, a handheld Microtops-2 sun photometer was used at *Polarstern* during Leg 5, too.

The solar- and near-infrared irradiance spectrometer (COmpact RAdiation measurement System; CORAS) was added during Leg 3 with the return of daylight. During Leg 5, CORAS measured almost continuously and was calibrated with a calibration lamp on 29 August 2020 and 19 September 2020 (also day of measurements end).

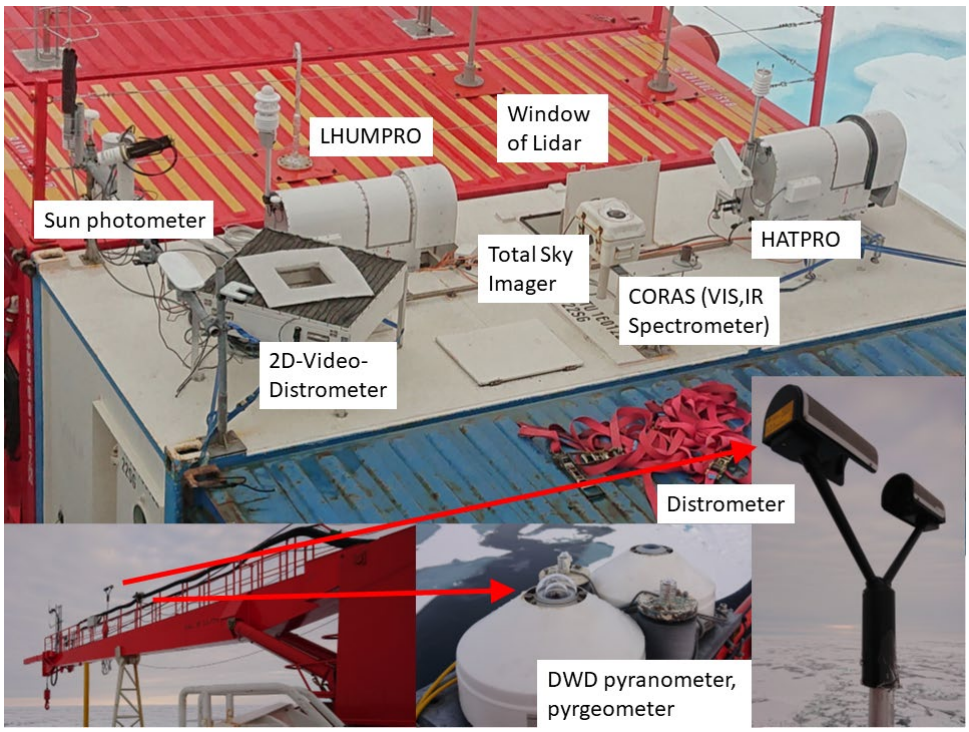

***Fig. 3.3.1**: Instruments on the roof of the Oceanet container and on the bow crane at the bow area of the Polarstern.*

All instruments had to be monitored for proper operation and several maintenance and calibration tasks were performed to ensure high data quality. The microwave radiometers operated continuously, except during calibration. HATPRO and LHUMPRO were calibrated with liquid nitrogen during the handover from Leg 4 to with Leg 5.

The lidar Polly^{XT} also operated continuously during Leg 5 until 2 October 2020, 0400UT. Gaps were only caused by maintenance work on the container roof as well as crane and helicopter operations above the OCEANET container.

The CIMEL sun photometer was repaired during the handover from Leg 4 to with Leg 5. But it could not be used for measurements later either due to low clouds and fog at the beginning of Leg 5 or due to low sun elevation angles later during Leg 5. Low sun elevation angles cause larger measurement errors and are not accepted by the automatic sun photometer algorithms. The handheld, non-automatically running Microtops-2 sun photometer could be operated at 6 days during Leg 5. A comparison to the ARM CIMEL sun photometer operated in vertical pointing “ship mode” could be of benefit but this comparison needs to take into account the atmospheric conditions of having often low clouds above the systems (ship) and having the sun slightly elevated above the horizon.

The Parsivel-2 laser disdrometer was installed on the bow crane on June 19 (Leg 4) and took measurements during the whole Leg 5 (until 2 October 2020, 0400UT). Its measuring principle,

its fixed position at the now crane, and the atmospheric conditions request further quality assurance of the data.

The 2DVD operated continuously until 2 October 2020, 0400UT.

The pyranometer and pyrgeometer continued to measure on the bow crane (until 2 October 2020 0400UT). This location is less affected by shading from the ships superstructure than the container roof. The installation of the Parsivel-2 laser disdrometer on the bow crane might have caused some shadings and needs to be regarded. Also icing has been observed at the pyranometer and pyrgeometer sensors partly. The sensors have been cleaned and re-levelled several times during Leg 5.

All measurements (except the standard meteorological measurements T, p, r.h.) were switched off due to the international regulations of not-performing measurements in the 12-mile zone of Norway around Svalbard on 2 October 2020, 0400UT.

The three wind (Doppler) lidars are employed on board *Polarstern* on the P-deck during Leg 5. The Halo Photonics Streamline lidar from the University of Trier and a Galion G4000 wind profiling lidar stayed at the starboard side (as during Leg 4), while the third wind lidar (Halo Photonics Streamline lidar from the University of Leeds) was put to the portside on 18 August 2020 to provide information about turbulence differences at the different ship sides. The Halo lidars provide measurements of backscatter intensity and along-beam Doppler velocity while the Galion provides only Doppler velocity as an output. All systems were operated independently until 2 October 2020 0400UT, each conducting a set of RHI scans at multiple azimuth angles, maximizing the information on boundary layer turbulent structure while minimizing the effort required by the instrument caretakers (compare cruise report Leg 1).

In addition to the technical setup and maintenance of the OCEANET instrumentation, an automatic profile retrieval algorithm for Polly^{XT} (dubbed Picasso) was used to make profiles of optical properties available in near real-time. This automatic dataset will be reanalyzed later according to PollyNET standards (Baars et al., 2016).

One of the main goals of this project is to link the aerosol information to cloud structure and radiative effects. For this purpose, we could make use of the preliminary data from the ARM KAZR cloud radar, the regular radiosoundings on board, and from the OCEANET lidar and microwave radiometer data and implement the Cloudnet algorithms (Illingworth et al., 2007). In this way, synergistic products, like classification masks and microphysical retrievals, could already be derived shortly after the measurements. All quicklooks were made available within *Polarstern's* internal network.

Preliminary (expected) results

Leg 5 was dominated by low overcast or fog conditions (e.g., Figs. 2 and 3) largely preventing full tropospheric lidar profiling. A first assessment of profiles at clear sky conditions showed that pronounced upper tropospheric aerosol layers were less frequent than during previous legs. In depth analysis of the lidar profiles still needs to be done.

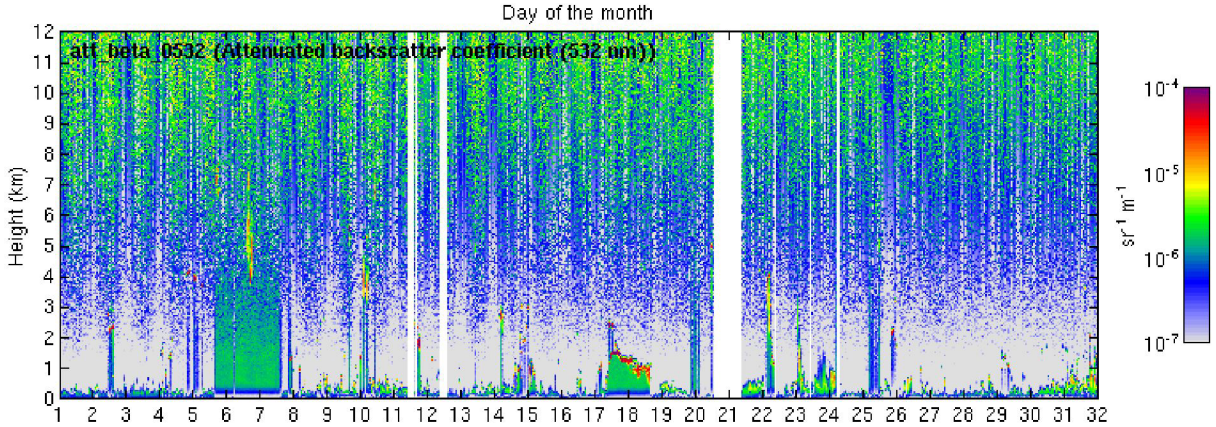

***Fig. 3.3.2**: Temporal development of the attenuated backscatter coefficient at 532 nm during August 2020 measured by OCEANET Arielle PollyXT lidar on the bow of Polarstern.*

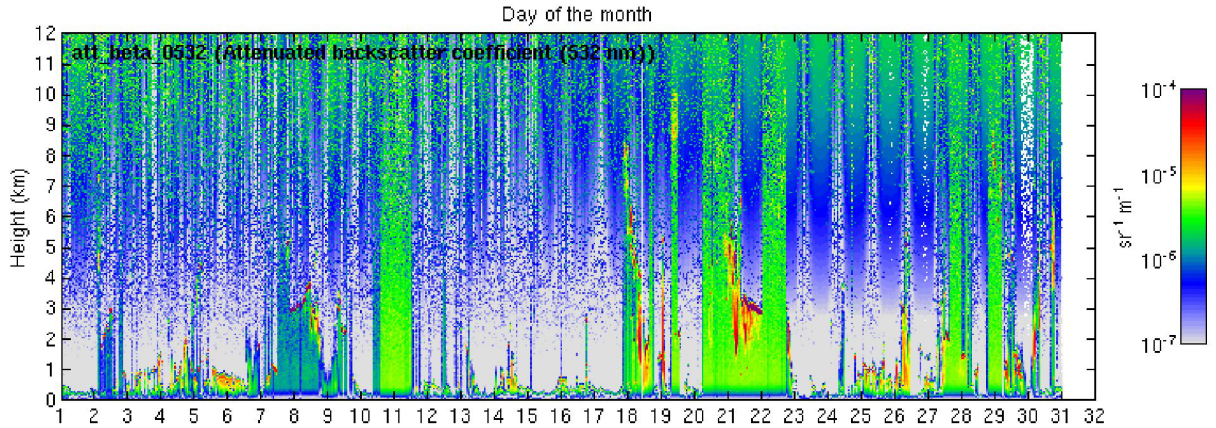

***Fig. 3.3.3**: Temporal development of the attenuated backscatter coefficient at 532 nm during September 2020 measured by OCEANET Arielle PollyXT lidar on the bow of Polarstern.*

Several low-pressure systems passed the measurement area during Leg 5. The permanently measured quantities integrated water vapor and the liquid water path (measured by the microwave radiometers) provide additional information to the atmospheric conditions as the change with the advection of air masses with different temperatures. Figs. 4 and 5 show an example of the change of these quantities.

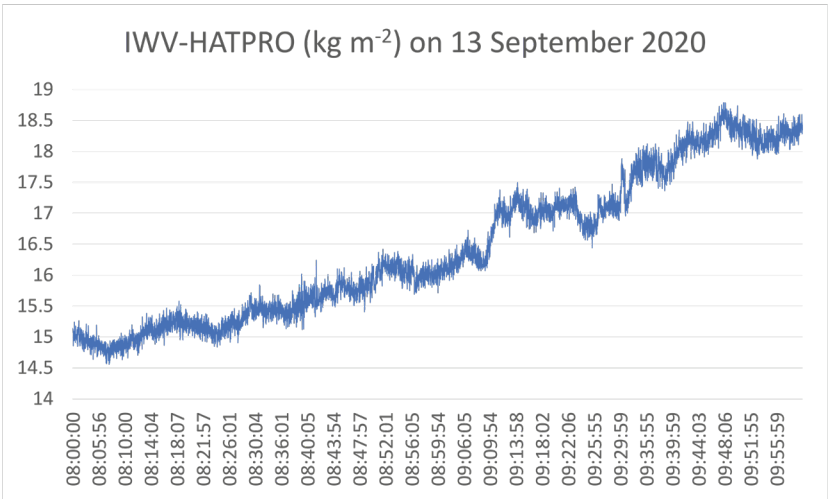

***Fig. 3.3.4**: Temporal development of the integrated water vapor on 13 September 2020, 0800-0959 UT measured by OCEANET HATPRO on the bow of Polarstern.*

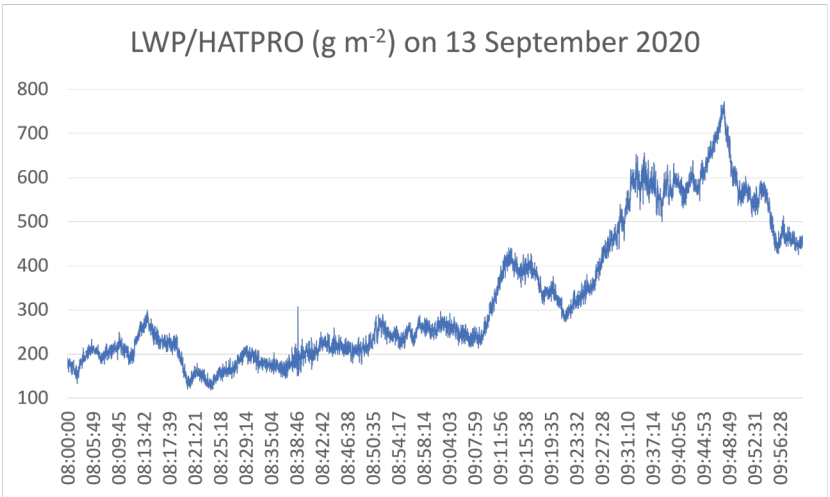

***Fig. 3.3.5**: Temporal development of the liquid water path on 13 September 2020, 0800-0959 UT measured by OCEANET HATPRO on the bow of Polarstern.*

Data management

All data are handled, documented, archived and published following the MOSAiC data policy (see APPENDIX). The raw data from the OCEANET platform are stored in the MCS following the MOSAiC data policy. The Polly^{XT} lidar data and quicklooks will be processed and made available through PollyNET (http://polly.tropos.de). Data will be stored at the PANGAEA data repository (World Data Center PANGAEA Data Publisher for Earth & Environmental Science www.pangaea.de).

References

Baars, H. et al. (2016) An overview of the first decade of PollyNET: an emerging network of automated Raman-polarization lidars for continuous aerosol profiling, Atmos. Chem. Phys., 16, 5111–5137.

Bohlmann, S. et al. (2018) Ship-borne aerosol profiling with lidar over the Atlantic Ocean: from pure marine conditions to complex dust–smoke mixtures, Atmos. Chem. Phys., 18, 9661–9679.

Engelmann, R. et al. (2016) The automated multiwavelength Raman polarization and water-vapor lidar PollyXT: the neXT generation, Atmos. Meas. Tech., 9, 1767–1784.

Illingworth, A.J. et al. (2007) CloudNet: Continuous evaluations of cloud profiles in seven operational models using ground-based observations, Bull. Amer. Meteor. Soc., 88, 883-898.

Kanitz, T. et al. (2013) North-south cross sections of the vertical aerosol distribution over the Atlantic Ocean from multiwavelength Raman/polarization lidar during Polarstern cruises, J. Geophys. Res. Atmos., 118, 2643-2655.

Kanitz, T. et al. (2011) Contrasting the impact of aerosols at northern and southern midlatitudes on heterogeneous ice formation, Geophys. Res. Lett., 38, L17802.

Yin, Z. et al. (2019) Aerosol measurements with shipborne sun-sky-lunar photometer and collocated multiwavelength Raman polarization lidar over the Atlantic Ocean, Atmos. Meas. Tech., in press.

3.4. ATMOSPHERIC SURFACE FLUXES FOR UNDERSTANDING SEA-ICE THERMODYNAMICS AND DYNAMICS

Ola Persson[1,2], Michael Gallagher[1,2], Roberta Pirazzini[7]

(not on board:) Matthew Shupe[1,2], David Costa[1,2], Thomas Ayers[2], Christopher Cox[2], Christopher Fairall[2], Daniel Gottas[2], Jesse Leach[2], Sara Morris[2], Jackson Osborne[1,2], Sergio Pezoa[2], Taneil Uttal[2], Ian Brooks[3], Jennifer Hutchings[4], Don Perovich[5], Timothy Stanton[6]

[1]EDU.CU
[2]GOV.NOAA
[3]UK.UNI-LEEDS
[4]EDU.ORSU
[5]EDU.DARTMOUTH
[6]EDU.NPS
[7]FI.FMI

Objectives:

This project is designed to examine the Surface Energy Budget (SEB) and how it impacts the sea-ice thermodynamic and dynamic processes that control the state of the ice over a full year. The PS122/5 collection period captured the synoptically-driven episodic freeze-melt cycles that characterize the onset of freeze at the end of the summer melt season at the new MOSAiC floe in the Central Arctic. The establishment of the ice camp on the new floe occurred after some surface freeze of melt ponds had already occurred, though a subsequent warm-air intrusion led to additional melt. An additional freeze and snowfall then occurred, followed by a brief melt with a warm intrusion including a rain-on-snow event, before renewed freeze occurred towards the end of the measurement period. These freeze-melt-freeze cycles had slightly different timing on the three primary surface types: bare ice, melt ponds, and leads. Ice movement forced by synoptic events modulated the extent of the leads and their freeze-up. In combination with partner MOSAiC projects, the overarching project objectives include:

(a) Build comprehensive atmospheric SEB, sea ice energy, upper ocean heat, and sea-ice momentum budgets; examine how these co-vary in space and time over all seasons of the year; and develop temporally-evolving process relationships among multiple key parameters.

(b) Use detailed field observations and a coupled regional model to examine how energy transfer processes (thermodynamics) are influenced by sea-ice deformation (dynamics) on sub-seasonal to seasonal time scales.

(c) Assess sea-ice predictability related to dynamic and thermodynamic process relationships, using a full year of quasi-operational, 10-day sea-ice forecasts.

In support of these broad project goals, the specific objectives of the SEB Flux team during PS122/5 was to obtain surface energy budget measurements over the primary surface types during the autumn freeze-up period in the central Arctic by deploying the two remaining ASFS sleds and establishing a new Central Observatory on the sea ice. This included redeployment of a collaborator-provided upper-ocean buoy recovered from an L-site abandoned in the Fram Strait, and the encouragement of the deployment of ice-measurement instrumentation and manual ice and upper-ocean measurements by other MOSAiC partners in the vicinity of the new Met City and the ASFS installations. Different timings of the SEB evolution were noted over the different surface types, motivating instrument deployment decisions and interdisciplinary coordination to better sample this spatio-temporal heterogeneity. The team also provided partial operational support for a number of related guest programs that did not have representatives on-board during PS122/5.

This project is funded by the US National Science Foundation and the US National Oceanic and Atmospheric Administration.

Work at Sea

Work during PS122/5 for the SEB Flux Team had 3 components: (1) Deploy and maintain two Atmospheric Surface Flux Stations (ASFS) at key locations within the new Central Observatory and in conjunction with complementary ice and upper ocean measurements; (2) Re-establish a Met City domain for the new Central Observatory including installation of the 11m tower; and (3) Installation and maintenance of several partner projects at various locations. An additional objective for Leg 5 was to characterize the heterogeneity of the SEB during freezeup using these assets and partnering with other MOSAiC researchers. PS122/5 started on 13 Aug with an ice reentry transit of the Polarstern from the rendezvous with the Akademik Tryoshnikov in the Fram Strait to the location of a new central Arctic ice floe found near 87.7° N, 105° E on Aug 21. The voyage was relatively quick because of a swath of low ice concentration extending north of Greenland nearly to the North Pole. PS122/5 ended with an exit transit towards Svalbard, leaving the drift floe on Sep 20 and arriving in Svalbard on Oct 2. On-board measurements continued along the exit transit; limited on-ice atmospheric measurements with the two ASFS sleds were also obtained at three ice stations. All parameters measured, including their installation location, are outlined in Table 3.4.1.

Atmospheric Surface Flux Stations

Both Atmospheric Surface Flux Stations (ASFS30 and ASFS50) were recovered from the ice at the end of Leg 4, and were operational and ready to be deployed from the working deck of the Polarstern for Leg 5. Because there was concern that freeze-up had already started on the day we arrived at our floe, the ASFS were put out by a team of volunteers immediately as sites were identified at the new Central Observatory (CO) floe (Fig 3.4.1). ASFS50 was put at the far southeastern end of the CO at the edge of a lead that defined the boundary of the floe, while ASFS30 was deployed at the southwestern corner of the floe which had been identified as the new Met City site. ASFS50 remained at its initial site through the entire floe drift until Sep 19, making observations as the ice froze and melted and the lead opened wider, froze, and closed with ridging. ASFS30 obtained SEB measurements at the Met City site during the time that MC instrumentation and infrastructure was deployed. MC was finally fully operational on Aug 27; ASFS30 remained at its MC location until Sep 4 while obtaining redundant overlapping data that could be used to extend the Met City SEB measurements as far back as

Fig. 3.4.1: Rapid deployment of ASFS50 at the Leg 5 CO floe on Aug 21, 2020. The ASFS sleds were very mobile and could be handled easily by 3 people (Photo: L. Nixon).

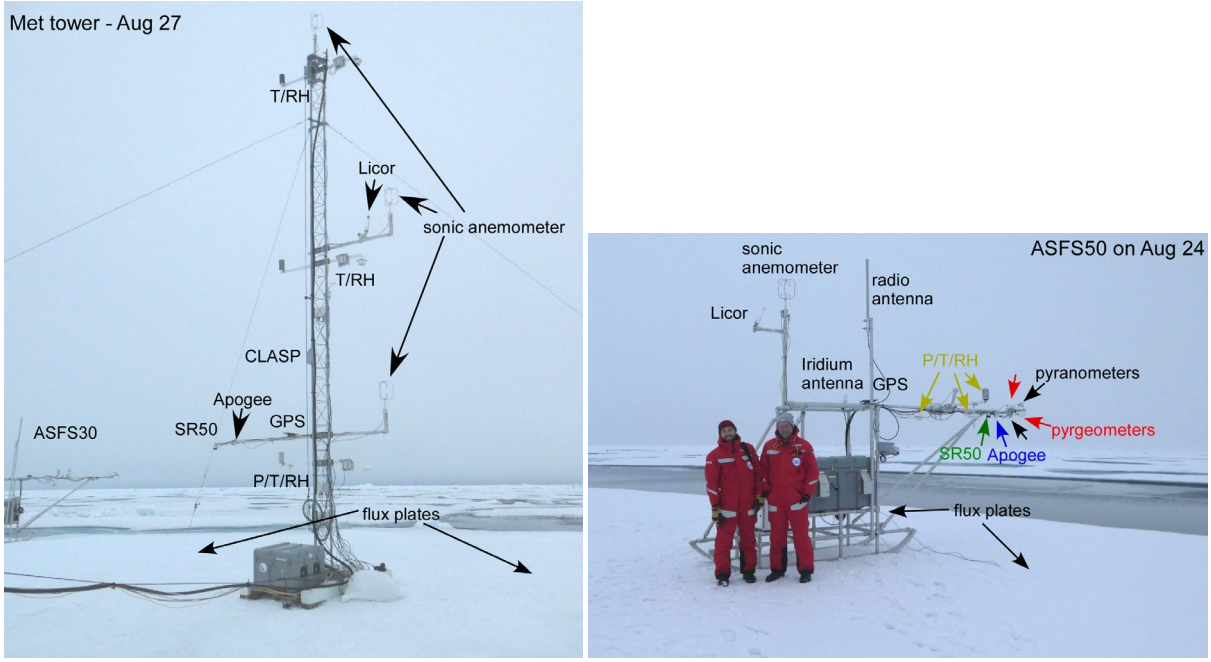

Fig. 3.4.2: (left): View looking SSW at the Met tower and ASFS30 shortly after raising of Met tower; (right) ASFS50 3 days after installation at lead site in the Central Observatory (Photos: O. Persson).

Aug 21. During this time, it had been noted that the freeze-up was occurring at a different rate over the different surface types, so, on Sep 4, ASFS30 was placed in a melt pond that had essentially not yet frozen (it had a very thin skin of ice on its surface). The placement of ASFS30 was also coordinated with the deployment of the two AWI sledges to produce a "stress line." This "stress line" would yield turbulent flux measurements from a ridge site and into the flatter, melt-pod covered, refreezing FYI, which should show the surface stress effects (form drag) of this large ridge for northerly wind conditions. ASFS30 remained at its Hinterland Pond site measuring the pond freeze-up until Sep 19, when both ASFS sleds were brought to the remote sensing site and lined up alongside the two AWI turbulence sledges to obtain 10 hours of intercomparison data. This intercomparison was essential to ascertain whether differences between the sleds and sledges during the floe drift time period were spatially-related or instrument-related.

The ASFS30 data showed significantly different energy budget evolution than the ASFS50 data, indicating that some of the spatial heterogeneity during the drift period was quantified by these deployments. Preliminary FMI radiation data from a Met City melt pond also suggest radiative differences (see below). The met tower turbulent heat fluxes and the ARM Met City radiation data have not yet been analyzed. Infrared helicopter mapping of nearby floes suggests significant temperature variability among meltponds, as well as between meltponds, leads and FYI areas.

During the exit transit, the ASFS sleds were utilized at the three ice stations, each lasting about 6 hours, to 1) further quantify the spatial variability of SEB terms over different surfaces along a "slow transect" line in coordination with detailed surface characterization measurements from Team Ice, 2) obtain additional SEB time series during the latter part of the freeze-up period, and 3) obtain estimates of the surface longwave, broadband emissivity value that is key for our SEB measurements. The emissivity is obtained by a Team Ice member (R. Pirazzini) making independent skin temperature measurements with a fine probe at the various slow transect measurement sites. The slow transect methodology was tested and revised at ice station 1, with ASFS50 deployed as a fixed-site control of the temporal evolution of the SEB during ice stations 2 and 3.

Consideration was also given to deploying the two ASFS sleds in a larger triangular array with Met City, with the nodes being separated by distances of ~15 km. The scientific purpose

would have been to obtain not only SEB measurements on different ice types, but also obtain measurements of the atmospheric divergence/deformation field hypothesized to directly impact the ice divergence/deformation. This was the original design and deployment during Leg 1 in conjunction with the large number of additional ice-based buoys, and the hope had been to retain this distributed network configuration through the entire MOSAiC year. However, with the melt-out of the original CO and the loss of the surrounding distributed network of buoys, the deployment of the ASFS sleds to more remote sites for these dynamic objectives became a lower priority, especially compared to capturing the spatial heterogeneity of the SEB during freeze-up. While such a redeployment could possibly have been done in early September when Met City was fully operational, it also had become clear that the prevailing low cloud/fog/icing conditions greatly curtailed any helicopter flights, that at most 2 weeks of data would have been acquired, that it was highly unlikely that any maintenance could be done at the sites during their deployment, and that there was a significant risk that at least one sled might not be recovered at the end. Hence, it was decided to keep ASFS50 at the lead site and redeploy ASFS30 to the melt pond site to obtain good measurements of the SEB heterogeneity in the CO vicinity where daily maintenance could be done.

Met City

Immediately upon arriving at the new floe on Aug 21, ASFS30 was placed at the site selected for the new Met City. The site selected for the tower was an old ridge that had thick ice (> 2m), though the area was surrounded by several melt ponds and was bounded by a lead to the SW through NW. The infrastructure installation and instrumentation of Met city continued over the next few days, with instrument comparisons on a reclining met tower starting on Aug 25 and culminating in the raising of the met tower on Aug. 27 (Figs. 3.4.2 and 3.4.3; Note: the met tower is labelled as the “10m Mast” in Fig. 3.4.3). To provide scale and orientation, the Met hut is ~15 m from the met tower, and the tower-to-hut direction was initially due north, but at the time of this image, aligning along 30° due to floe rotation (see Fig. 3.4.4). Additional atmospheric instrumentation at Met City included the ARM radiation sensors (Swing Set, IceRad), precipitation gauges (Precip, Parseval), and present weather detector (PWD);

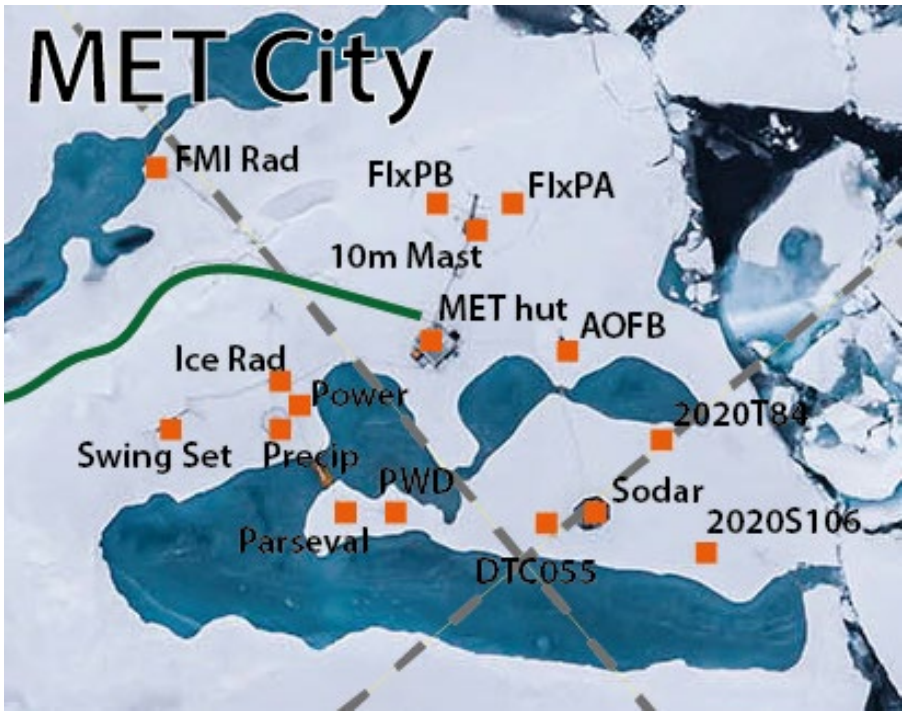

Fig. 3.4.3: Met City installation names placed on a drone-acquired photograph

the FMI radiation sensors; and the ULeeds sodar. Later additions included the Naval Post-graduate School AOFB (upper ocean buoy), and two thermistor strings (DTC055, 2020T84) and a snow-ice mass balance buoy (2020S106) courtesy M. Hoppmann (AWI).

Once the ARM and FMI radiation and the flux tower data came on-line and characterized the SEB at Met City, ASFS30 became redundant and was moved on Sep 4 (see sections 3.4 and 3.7). (Note: Fig. 3.4.3 was taken after ASFS30 was moved. It had been located on the flat ice just above and to the right of the "d" in "FMI Rad"). Because of strong surface melt on Aug 28, snow/ice from the AOFB hole was piled around the tower base to prevent further melt. On Sep 8 (~11 UTC), a large ~1.5 m high, ice block moved up on the Met City floe at the very top of the Fig. 3.4.3 image along the melt pond and lead edges to the south of the met tower. This weight likely caused the subsequent 3-4 cm wide crack in the ice running in a 70-m long arc from SE to NW between the met tower and the met hut. While of concern, this crack fortunately did not change during the rest of the Met City deployment. The increased roughness is clearly seen in, for example, the turbulent kinetic energy data for southerly winds after this event.
Surface energy budget calculations will be done using both the ARM and FMI broadband radiation data, along with the turbulent sensible and latent heat fluxes calculated from the met tower instruments. The ARM "Swing Set" (upwelling radiation) was installed on an untrampled ice surface with no significant view of any of the meltponds. Radiation from this site should provide excellent data for ice-only surfaces, as in contrast to the FMI and ASFS radiation sensors. Skin temperature and snow depth were also obtained by sensors on the met tower, with occasional manual snow depth observations after snowfalls made to calibrate the automated values from the SR50 instrument. The flux plates were placed near the base of the tower and the area marked as a "no go" zone. The flux plates did melt out after the first warm period, but were again covered by subsequent snowfalls. The two were surprisingly consistent with each other. Daily visits were made to clean instruments within reach when necessary, and to document changes with numerous photographs. Icing from freezing fog was a problem for the Licor (and pyranometers) during the first 10 days of the Met City deployment, becoming less of an issue during the 2nd half of the deployment. The Licor heating helped remove icing once riming conditions stopped and temperatures got colder.

The ice at Met City did move during the floe drift period, even relative to the Polarstern. During the drift, the met tower averaged about 386 m from the *Polarstern*, ranging between 340 and 440 m, and the floe turned clockwise about 35 degrees, most of it up until Sep 6 (YD250) (Fig. 3.4.4). Tidal oscillations are evident in this data. Relationships to near-

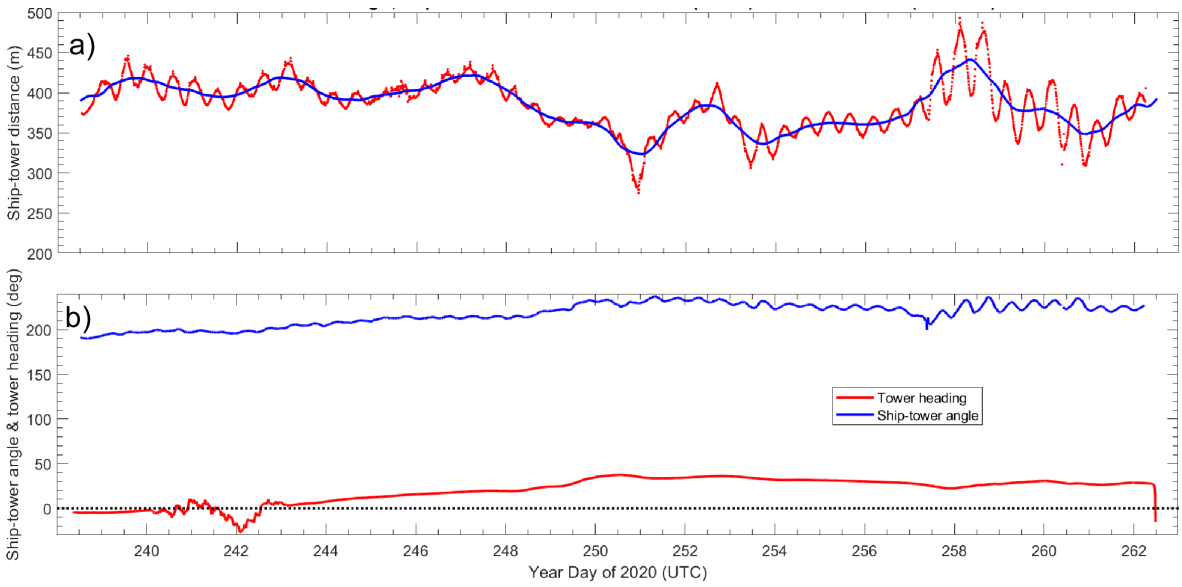

Fig 3.4.4: Time series from Met City of a) ship-met tower distance and b) tower heading (red) and ship-tower angle (blue). The blue line in a) represents a 24-h running mean of the 10-min data in red.

surface winds are likely and will be explored. Met City was dismantled on Sep 18 after having had ~22 days of measurements. Quick-look figures suggest the data to be of high quality with only two short power outages of less than 2 h each, one due to an inquisitive bear.

Support for Partner Projects

During operations of Leg 5, the University of Colorado / NOAA flux team supported the operations of a number of other collaborators whose instruments provide complementary information towards achieving shared scientific objectives. These include:

- SODAR (PI: Ian Brooks): The University of Leeds sodar system is designed to measure wind profiles over the lowest 200-400m. It was set up at Met City starting on 26 Aug and was operational until Sep 18. This system was to the NW of the Met Hut on an ice island in another Met City meltpond (see Fig. 3.4.3). The system was leveled and oriented such that the system's NE-to-SW corners were pointed directly at the bridge of Polarstern, with SW away. The north side of the system was pointed to approximately 350 degrees upon installation. On Aug 28, a small crack developed underneath the sodar enclosure and transmitter. Both were moved about 4 meters to the east and the system restarted. Two snowfalls required cleaning of the transmitter. The sodar operated consistently when there was power provided to Met City, routinely showing wind profiles on its laptop up to multiple 100s of meters.
- ULeeds HALO Lidar (PI: Ian Brooks): The University of Leeds Halo scanning lidar system had been deployed on the ice floe in earlier legs in order to obtain wind profiles, turbulence data, and "virtual tower" data. After the floe was abandoned at the end of Leg 3, it was moved to the P-deck of the Polarstern and run in VAD mode next to the ULeeds Galeon lidar, also running in VAD mode. At the request of PI Brooks early in Leg 5, CU, ARM, and TROPOS members moved this lidar to the port-side railing and installed a partial RHI scanning routine to complement the UTrier scanning Halo lidar on the starboard-side railing. The purpose was to obtain turbulence profiles in the boundary layer in as many wind conditions as possible. The new installation and new scanning routine was operational on Sep 6. The system ran continuously until instruments were turned off upon entry of Svalbard waters on Oct 2.
- FMI-Radiation (PI: Roberta Pirazzini): On other legs, a radiation suite from the Finnish Meteorological Institute was designed to measure the upwelling, downwelling, longwave and shortwave radiation, including the partitioning of direct and diffuse shortwave radiation (SPN1 sunshine pyranometer). Since Dr. Pirazzini was present on Leg 5 and after consulting with the CU team, she set up this system with the downward facing instruments located over one of the Met City meltponds (see Fig. 2). As this system is prone to ice over and Dr. Pirazzini often had obligations elsewhere in the CO, the ARM and sometimes CU team performed daily maintenance of this system and documented changes in the evolving surface characteristics with photographs. The station operated without breaks from Aug 28 until Sep 18.
- Snow Particle Counters and CLASP (PI: Markus Frey). The British Antarctic Survey provided sensors for installation on the 11m tower to measure blowing snow particles and aerosols. The CLASP was operated at approximately 3m height and operated between Aug 27 and Sep 18. Both SPCs and data cards were not initially found when the tower was raised, but were later located and the SPCs installed at about 30cm and 10m on Aug 31 (see Figure 3.4.4). Several snowfall events did occur during Leg 5, potentially providing data for the SPCs. However, SPC data was only collected on the data cards, as the communication system did not have connection to the data logging system. Data has not been pulled off these cards to be stored on the CU data logging system, nor has the data been sent to the MCS. Hence, the amount and quality of the data for Leg 5 is unknown. The lowest SPC might have been impacted by low-level turbulence and flow distortion around the base of the tower.

- Ice Video Camera System (PI: Max Maahn): The VISSS takes high resolution, rapid succession photographs of falling ice crystals, and was installed at the end of Leg 3 on the Observation Deck of Polarstern to provide stability for longer term operations. In this position it could suffer from potential flow distortion on the trajectory of falling precipitation, but would not be challenged by cracking and moving ice on the surface. Operations were conducted during Leg 5, and several snowfall and two rain events could have provided data.
- Distributed Network: Across the Distributed Network key partners have installed equipment that is very relevant for our understanding of the surface energy budget, energy fluxes to the sea ice, and more. Most of that equipment was lost when the old MOSAiC floe melted out and the old CO abandoned at the end of Leg 4. The Arctic Ocean Flux Buoy (AOFB) recovered from L2 during Leg 4 was reinstalled at Met City during Leg 5. The Acoustic Doppler Current Profiler (ADCP) unit on the AOFB had been damaged and was non-functional, and was saved for shipment back to PI T. Stanton (NPS). In addition, the carriage for the turbulence sensor was also non-functional and was not repairable despite significant efforts by Leg 5 members. The crack in the downward-facing radiometer was repaired, but likely not functional. The AOFB that was installed at Met City had an operational turbulence sensor that was fixed at the bottom depth of the carriage and an operational upward facing radiometer. Communications with T. Stanton (NPS) confirmed that the unit was sending data. AOFB44 was installed first on Aug 30, briefly removed and reinstalled on Sep 10 to attempt further repairs. It was left at the floe when the exit transit began on Sep 20, still sending data via Iridium.

Variable	**Instruments**	**Installation Locations**	**Details**
Surface Conductive Heat Flux (at ice snow interface)	Hukseflux Flux plates	Near 11m tower at Met City (2)	Plates were initally buried under a few cms of surface scattering layer „snow“. They then melted out and were re-covered by real snow. Data looks reasonably but must be carefully considered. Daily photgraphs.
		ASFS50 at lead area (2)	Plates installed under new snow on Aug 24, 3 days after sled deployment. Plates installed as stationary control at IS 3.
		ASFS30 initially at MC (Aug 21); moved to Hinterland Pond Sep 4 (2)	Initially as for ASFS50; once at Hinterland, plates not installed at first because surface was liquid. After some surface freeze, plates show large temporal fluctuations and variability between the two. Numerous photos show variability of snow cover & freezing into ice. Careful

			physial consideration of values necessary.
P, T, RH – 2m	Vaisala PTU337	11m tower at Met City	Operated continuously from 25 Aug through 18 Sep.
		ASFS50 at lead area; also at Ice Station 2 & 3	Operated continuously from 21 Aug through 20 Sep. Was stationary control at IS 2 & 3.
		ASFS30 at MC Aug 21-Sep 4; in Hinterland Pond Sep 4- 19. Also at Ice Stations 1, 2, & 3 (Sep 24, 26, 30).	Obtained initial MC SEB data; then became redundant & moved into Hinterland Pond to sample a pond freeze-up. Performed „slow transects“ at IS 1, 2, & 3.
T, RH – 6m & 10m	Vaisala HMT307	11m tower at Met City	Operated continuously from 25 Aug through 18 Sep
Fast response winds – 2m, 6m, and 10m	Metek Sonic anemometer	11m tower at Met City	Operated continuously from 25 Aug through 18 Sep
Fast response winds – 3m	Metek Sonic anemometer	ASFS50 at lead area; also at Ice Station 2 & 3	Operated continuously from 21 Aug through 20 Sep. Was stationary control at IS 2 & 3.
		ASFS30 at MC Aug 21-Sep 4; in Hinterland Pond Sep 4- 19. Also at Ice Stations 1, 2, & 3.	Obtained initial MC SEB data; then became redundant & moved into Hinterland Pond to sample a pond freeze-up. Performed „slow transects“ at IS 1, 2, & 3.
Fast water vapor and carbon dioxide – 6m	LICOR open path gas analyzer	11m tower at Met City	Operated continuously from 25 Aug through 18 Sep. Periodic data degradation due to icing on sensor. Heater sometimes removed this.
Fast water vapor and carbon dioxide – 3m	LICOR open path gas analyzer	ASFS50 at lead area; also at Ice Station 2 & 3	Operated continuously from 21 Aug through 20 Sep. Was stationary control at IS 2 & 3. Occasional data degradation due to icing on sensor, but manually cleaned when noted.
		ASFS30 at MC Aug 21-Sep 4; in Hinterland Pond Sep 4- 19. Also at Ice Stations 1, 2, & 3.	Obtained initial MC SEB data; then became redundant & moved into Hinterland Pond to sample pond freeze-up. Performed „slow transects“ at IS 1, 2, & 3.

Position and Heading, 2m	Hemisphere dual GPS	11m tower at Met City	Operated continuously from 25 Aug through 18 Sep.
		ASFS50 at lead area; also at Ice Station 2 & 3	Operated continuously from 21 Aug through 20 Sep, and for IS 2 & 3
		ASFS30 at MC Aug 21-Sep 4; in Hinterland Pond Sep 4- 19. Also at Ice Stations 1, 2, & 3.	Obtained initial MC SEB data; then became redundant & moved into Hinterland Pond to sample pond freeze-up. Performed „slow transects“ at IS 1, 2, & 3.
Surface height (snow depth, ice melt)	Campbell SR50 sonic ranger	11m tower at Met City	Operated continuously from 25 Aug through 18 Sep.
		ASFS50 at lead area; also at Ice Station 2 & 3	Operated continuously from 21 Aug but stopped working on ?? Sep; reason never found
		ASFS30 at MC Aug 21-Sep 4; in Hinterland Pond Sep 4- 19. Also at Ice Stations 1, 2, & 3.	Operated continuously from 21 Aug but stopped working and was replaced with spare on Sep 13; reason never found for failure.
Infrared Surface Temperature	Apogee IRT	11m tower at Met City	Operated continuously from 25 Aug through 18 Sep. Seemed to measure early ice melt, and captured snowfall events.
		ASFS50 at lead area; also at Ice Station 2 & 3	Operated continuously from 21 Aug through 20 Sep, and for IS 2 & 3
		ASFS30 at MC Aug 21-Sep 4; in Hinterland Pond Sep 4- 19. Also at Ice Stations 1, 2, & 3.	Obtained initial MC SEB data; then became redundant & moved into Hinterland Pond to sample pond freeze-up. Performed „slow transects“ at IS 1, 2, & 3.
		On P-deck starboard-sdie railing pointed at ~ 45 deg angle towards surface (Aug 17-Oct 2)	Obtain Tskin along ship track during reentry and exit transits; estimate LWu, possibly Hs, Hl, and surface type. Also to note freeze-onset. Occasionally rimed or ice-coated. Partially neglected while at floe, but maintained during both reentry and exit transits.

Radiation: SW, LW, up and down, 2m	Hukseflux radiation suite	ASFS50 at lead area; also at Ice Station 2 & 3	Operated continuously from 21 Aug through 20 Sep, and for IS 2 & 3. Pyranometers sometimes iced/frozen-cleaned daily. PIRs nealy always clear
		ASFS30 at MC Aug 21-Sep 4; in Hinterland Pond Sep 4- 19. Also at Ice Stations 1, 2, & 3.	Obtained initial MC SEB data; then became redundant & moved into Hinterland Pond to sample pond freeze-up. Performed „slow transects“ at IS 1, 2, & 3. Pyranometers sometimes iced/frozen-cleaned daily. PIRs nealy always clear
Radiation: SW, LW, up & down, SW diffuse & direct	Radiation Station (FMI)	Near MC meltpond	Operated continuously from Aug 28 - Sep 18. Some data quality issues related to tilting of radiation stand and riming/icing, though maintained daily by ARM. Captured meltpond albedo evolution.
Aerosol size distribution – 3m	CLASP (BAS)	11m tower at Met City	Operated continuously from 27 Aug through 18 Sep.
Snow Particle Counts – 0.3 and 10m	SPC (BAS)	11m tower at Met City	Operated continuously from 31 Aug through 18 Sep.
Wind Profiles (u,v,w up to about 400m)	SODAR (U. Leeds)	Near Met Hut	Operated continuously from 26 Aug through 18 Sep.
Ice Crystal Precipitation Images	VISSS (U. Colorado)	Polarstern Observation deck.	Operated continuously through Leg 5.

Table 3.4.1 Parameters measured and systems maintained by the SEB/Flux team during Leg 5. “Near continuous” measurements at Met City means that the measurements were operational except for the relatively short power outages that occurred on two occasions.

Preliminary (expected) results

Measurements made as part of this project have extended important timeseries that include high-quality estimates of atmospheric surface heat and momentum fluxes at multiple locations across the MOSAiC domain and the lower atmosphere structure at the MOSAiC Central Observatory. Ultimately these fluxes will be combined with project partner measurements of ocean heat fluxes, sea ice thermodynamic state and thickness, and regional-scale sea-ice movement and deformation to understand the dynamic and thermodynamic drivers of the sea-ice life cycle. While there are many expected results and applications of the

data, a few are highlighted here to demonstrate the detail and breadth of the obtained data sets.

The first area of focus is the autumn freeze-up. Autumn freeze-up over Arctic sea ice areas have known to occur as early as Aug 20, so establishing on-ice SEB sites needed to be done quickly after leaving the Tryoshnikov. The Apogee IR thermometer installed on the ship's P-deck starboard railing to monitor the skin temperature along the Polarstern's track is one source of data that can be used to determine the extent of freeze-up and obtain an estimate of the SEB along the reentry transit. There was concern that the permanent freeze-up transition had already occurred during the reentry transit before the Polarstern's arrival at the new CO floe on Aug 21, as many meltponds had a thin layer of ice at that time. However, as new warm-air advection introduced warm, moist air aloft, enhanced downwelling longwave radiation resumed the surface melt Aug 23-24 and then more strongly on Aug 26 - Sep 2. A preliminary net atmospheric energy flux (F_{atm}) calculation at both ASFS30 and ASFS50, calculated using ASFS measured radiation data and bulk turbulent heat fluxes, was in the range of +10-40 W m^{-2} through Sep 2, with only some hours on Aug 24-25 being negative (~-25 W m^{-2}). This scenario is consistent with the observations of melt pond ice disappearance and size increases and a negative change in the "snow depth" at Met City, though further analysis and calculations using covariance turbulent fluxes and the ARM radiation data at Met City are needed to confirm this scenario. Starting on Sep 4, preliminary F_{atm} calculations for ASFS50 became consistently negative until departing the ice floe on Sep 20, except for less than 24 hours of positive values on Sep 12-13 as temperatures aloft again warmed to above freezing, in advance of a complex Arctic cyclone with a rain-on-snow period on Sep 13-14 and some additional surface melt. Hence, this data suggest a temporary freeze-up before Aug 21, additional melt until Sep 2, significant freeze-up Sep 4-Sep12, a short 24 h melt period Sep 13-14, and a return to significant freeze Sep 14-20. Presumably, this last freeze was the permanent seasonal one lasting until spring, though our data can't show it. Melt-freeze-melt-freeze cycles are likely typical for the autumn freeze-up over Arctic sea ice.

Preliminary broadband radiometer data at Met City shows this melt-freeze-melt-freeze cycle as well, and is illustrated in photographs at the FMI radiometer site (Fig. 3.4.4). The radiometers were installed over a melt pond on Aug 28, with a low albedo of <0.4 which decreased for the next few days. These remained below 0.4 until Sep 4, when they increased rapidly to near winter values of 0.85 by Sep 10, then decreased again by 0.18 on Sep 14 with the brief melt and rain-on-snow event, and finally increased yet again to 0.80 at the end of the drift. Note that these data are very preliminary, have not been edited for effects of riming and other issues, and should not be considered final nor quoted.

During the periods with above-freezing air aloft, 10-min, 2-m temperatures at Met City (T_{2m}; preliminary, uncalibrated) were often a few tenths of a degree above freezing (Fig. 3.4.5). During Leg 5, the Met City T_{2m} temperatures were above freezing 23% of the time (though never higher than +0.9 °C), while below freezing 77% of the time. The lowest T_{2m} was -13.2 °C on Sep 11. The skin temperature was only slightly colder than the 2-m level most of the time, except when strong cooling occurred on Sep 7, 10, and 11. Strong surface inversions occurred at these times. The strongest winds occurred with the cyclone on Sep 13-14, reaching 13.8 m/s at the 10-m height, which was also the event with the lowest sea-level pressure of 989 hPa. Five cyclones passed close enough to produce local pressure minima. Several of them produced precipitation (both rain and snow), with a snowfall of 5-7 cm being produced by the cyclone on Sep 9. The cyclones on Sep 6-7 and 13-15 were declared as Intensive Observing Periods, and were sampled more intensively by all research teams. The atmospheric team enhanced soundings to 3-hourly during these IOPs. The significant melt with warm air aloft Aug 26-Sep 2 (YD239 - YD246) occurred primarily under high surface pressure.

Good turbulent flux measurements are anticipated from the met tower data set, as the wind rose shows the primary wind directions as being from the south, with a secondary frequency peak from the east (Fig. 3.4.7a). Turbulent flux data from ASFS50 is expected to be as good or even better, as both the south sector and a broad east sector were clear of unnatural

Fig. 3.4.5: *Temporal evolution of the surface conditions below the FMI broadband radiation station. Photos: R. Pirazzini.*

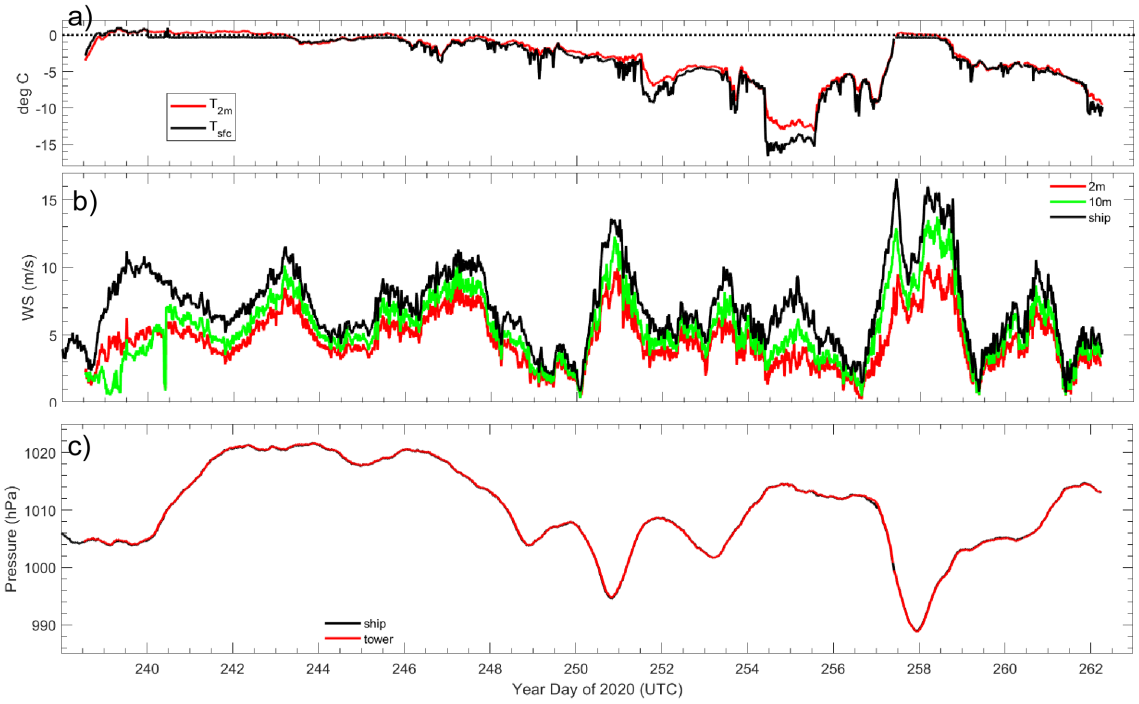

Fig. 3.4.6: *10-min average time series of preliminary data from the met tower at Met City showing a) 2-m (red) and skin temperature (black); b) wind speed at 2 m (red) and 10 m (green), and c) sea-level pressure (red). The black curves in b) and c) show the corresponding data from the ship weather station, with winds measured on the mast at 39 m above the water line. The raising of the met tower can be seen by the „spike“ in the 10-m wind speed near 11 UTC Aug 27 (YD240).*

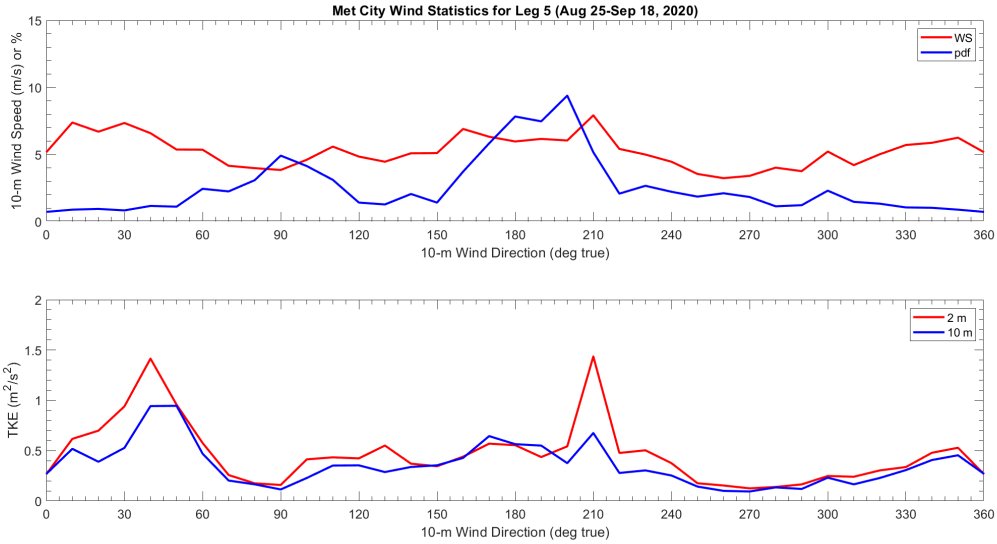

***Fig. 3.4.7**: a) Wind direction frequency(blue) and wind speed as a function of 10-m wind direction; b) turbulent kinetic energy as a function of wind direction for the 2-m (red) and 10-m (blue) heights on the sonic anemometer. Data from the entire floe drift period are used. Data are preliminary and may change with further analysis.*

structures. The main camp installations and the ship were located to the north through ENE wind sectors (see blue line in Fig. 3.4.4b), which only occur 12-15% of the time. Before Sep 8, the sector south of the met tower was primarily flat ice with meltponds and a small lead. On Sep 8, a block of ice was pushed up on the Met City floe about 20 m from the flux tower, producing a 3-4 cm crack under the guy wire between the met hut and the tower (this crack was of concern, but did not widen). The block transcended approximately a 30° sector with and was about 1.2 m high at its eastern end and 2.0 m high on its western end. It produced significant turbulence effects for all levels of the tower (Fig. 3.4.7b), especially at the 2-m level, for the 10 days after this date. Roughness calculations need to account for this feature.

Additional measurements were made during the exit transit that supplement this SEB work. At three ice stations, each ~6 hours long, ASFS30 was deployed in "slow transects" of ~300-400 m in length where 15-45 min stations along the transect spaced 25-80 m apart obtained the SEB over a variety of surfaces (snow-covered ice, frozen melt ponds with and without snow cover, thin frozen leads) and Team Ice made additional measurements of the surface to better understand the SEB impacts of detailed snow and ice structure. Furthermore, independent T_{skin} measurements were made under the radiometers to independently estimate the surface emissivity of the different surfaces, allowing an assessment of the value being used in our SEB studies. During ice stations 2 and 3, ASFS50 obtained continuous SEB data over one ice type to document the temporal variability during the slow transects.

Also during the exit transit, an Apogee IR thermometer, mounted on the starboard-side railing of the P-deck on *Polarstern*, obtained the skin temperature along the ship's track. This will aid in estimating the SEB along the track. This T_{skin} data is of particular interest during three ice edge transects done during the exit transit, where additional soundings, ship-based surface/upper-ocean, meteorological and boundary-layer lidar measurements, and vertically-pointing radar data will allow some documentation of the ice edge processes during freeze-up when the ice edge started to expand southward.

Data management

Data produced at the Met City installation are archived locally in Met City and duplicated in the flux laboratory container onboard *Polarstern*. Data produced at the remote ASFS sites are archived locally on the remote systems; some sub-set of this data is transferred to *Polarstern* via radio modems. The full set of ASFS site data is transferred to *Polarstern* after routine site

visits. All data is redundantly archived on the server in the flux laboratory container onboard *Polarstern*. Additionally, a copy of all raw data has been uploaded to the MOSAiC Central Storage onboard *Polarstern*; this data has not yet undergone detailed quality assurance and calibration. Long term archival of quality-controlled data will be done at the Arctic Data Center (ADC) archive, according to the protocol agreed upon between the ADC and PANGAEA. DOIs for the data will be communicated to PANGAEA for later access via the future MOSAiC Data Portal. All data are handled, documented, archived and published following the MOSAiC data policy. Exceptions will to be documented in written agreements between the data provider and the MOSAiC Project Board and data manager.

References

None.

Figure Captions:

Fig. 3.4.1: *Rapid deployment of ASFS50 at the Leg 5 CO floe on Aug 21, 2020. The ASFS sleds were very mobile and could be handled easily by 3 people (Photo: L. Nixon).*

Fig. 3.4.2*: (left): Met tower and ASFS30 shortly after raising of Met tower; (right) ASFS50 3 days after installation at lead site in Central Observatory (photos: O. Persson).*

Fig. 3.4.3*: Met City installation names placed on a drone-acquired photograph*

Fig 3.4.4*: Time series from Met City of a) ship-met tower distance and b) tower heading (red) and ship-tower angle (blue).*

Fig. 3.4.5: *Temporal evolution of the surface conditions below the FMI broadband radiation station. Photos: R. Pirazzini.*

Fig. 3.4.6: *10-min average time series of preliminary data from the met tower at Met City showing a) 2-m (red) and skin temperature (black); b) wind speed at 2 m (red) and 10 m (green), and c) sea-level pressure (red). The black curves in b) and c) show the corresponding data from the ship weather station, with winds measured on the mast at 39 m above the water line. The raising of the met tower can be seen by the „spike“ in the 10-m wind speed near 11 UTC Aug 27 (YD240).*

Fig. 3.4.7*: a) Wind direction frequency(blue) and wind speed as a function of 10-m wind direction; b) turbulent kinetic energy as a function of wind direction for the 2-m (red) and 10-m (blue) heights on the sonic anemometer. Data from the entire floe drift period are used. Data are preliminary and may change with further analysis.*

3.5 TRACE GAS FLUX & REACTIVE GASES

Byron Blomquist[2,3], Hélène Angot[2], Kevin Posman[1]

(not on board): Stephen Archer[1], Detlev Helmig[2], Christopher Fairall[3], Laurens Ganzeveld[4], William Sturges[5], Dean Howard[2], Ludovic Bariteau[2,3], Hans-Werner Jacobi[6], Sjoerd Barten[4], Lucy Carpenter[7]

[1]ORG.BIGELOW
[2]EDU.CU
[3]GOV.NOAA
[4]NL.WUR
[5]UK.AC.UEA
[6]FR.UGA
[7]UK.AC.YORK

Grant-Nos. NSF OPP 1807496 & NSF OPP 1807163 / NSF OPP 1914781

Objectives

This work encompasses two NSF-funded research projects focusing on air-sea exchange of climate-active trace gases and the atmospheric chemistry of reactive gases, respectively.

Air-sea exchange field work involves eddy correlation (EC) flux measurements of carbon dioxide (CO_2), methane (CH_4), ozone (O_3) and dimethyl sulfide (DMS) from a meteorological tower mounted at the end of the *Polarstern* bow crane. EC flux measurements of CO_2 and CH_4 are also conducted on the sea ice at the MetCity 10m meteorological tower. Additional, discrete flux measurements of CO_2, CH_4 and DMS are done over snow, ice and water surfaces with a dynamic-chamber flux measurement system.

Reactive gases field work is focused on continuous bulk concentration measurements of key reactive species (ozone, nitrogen oxides, volatile organic carbon and halocarbons, and gaseous elemental mercury). These samples are drawn from air inlets on the *Polarstern* bow crane. Additional compressed-flask air samples are collected on a weekly basis for post-cruise analysis of organic carbon and halocarbon species by our collaborators at UEA, and for CO_2/CH_4 by the NOAA GML Greenhouse Gas Monitoring program.

These field measurements form the basis for analysis and modelling of process-level gas transfer mechanisms in the sea ice environment and for modelling reactive trace gas budgets in the atmosphere.

Work at sea

Instrumentation deployed by this project for MOSAiC Leg 5 are listed in Table 3.5.1, including the SensorWeb short name for each device. Except for the flux chambers and flasks these are nominally continuous measurements, but there are periods of down-time due to instrument malfunction, maintenance, and unsuitable measurement conditions. Figure 3.5.1 shows a timeline for each continuous measurement indicating the periods of operation during Leg 5. Table 3.5.2 lists deployment dates for the dynamic chamber flux system, the species measured, and the surface type sampled. Text in the following paragraphs provides additional detail for each instrument and the measured quantities.

The two anemometers (*sonic_anemometer_3D_ship_bow*, *sonic_anemometer_2D_ship_bow*) are standard commercial instruments for wind speed measurement (Metek uSonic-3 Omni, RM Young model 86004), both installed on the bow tower with the 3D sonic at the top of the tower and the 2D sonic about 1.5m lower. The 2D sonic is used for a real-time wind display in the flux laboratory van on E deck. The 3D sonic is used for flux measurements. Gas sampling inlets for CO_2, CH_4, DMS and O_3 flux were located at the base of the 3D anemometer. The oritinal bow tower was broken during Leg 3. A shorter replacement tower was installed at the start of Leg 4. The 3D sonic height was ~20m ASL on the original tower and ~18m on the replacement tower. Gas fluxes from the MetCity tower are computed with wind data from the University of Colorado 10m sonic operated by the Univ. Colorado Shupe/Persson project.

The DMS analyser (*dms_apims_ship_bow*) is a custom-built Atmospheric Pressure Ionization Mass Spectrometer (APIMS) for fast (10Hz) measurement of the DMS concentration (Blomquist et al., 2010). It uses ion-counting to measure the principal ambient DMS isotopomer at mass 63. The ambient DMS concentration is obtained by reference to an isotopically labelled d3-DMS standard at mass 66, continuously added to the sample air stream at the inlet. The DMS concentration is computed using the raw count rates at masses 63 and 66, measured gas flow rates, and the known concentration of the d3-DMS internal standard. This instrument had an electronic failure during Leg 1 and did not operate during Legs 2-3. Following repairs on Leg 4 it resumed measurements on July 13.

The two Picarro greenhouse gas analysers (*crds_ghg_ship_bow*, *crds_ghg_ice_station_tower*) are commercial cavity-ring-down trace gas analysers specialized for fast, high flow-rate measurement of CO_2 and CH_4 flux (Picarro model G2311-f).

The chemiluminescent fast ozone analyser (*ozone_fast_ship_bow*) is a custom-built system measuring photons emitted by the reaction of ozone with nitrogen monoxide reagent gas (NO) (Bariteau et al.,2010). The ozone concentration is roughly calibrated, and a final calibration will be done post-cruise using reference concentration data from the slow ozone analyser.

The open path Licor (*licor_7500ds_ship_bow*) is a commercial instrument for fast measurement of water vapor and CO_2 (model 7500DS). This was installed on the bow tower, just below the 3D sonic and above the 2D sonic for measuring water vapor flux (latent heat flux). The 7500DS data are only usable when the optics are clean and dry. The CO_2 data from this instrument are not generally reliable for low-level flux measurements due to interferences.

The chemiluminescent NO/NO_2 analyser (*nox_ship_bow*) is a custom-built system operating on the same principle as the fast ozone instrument. In this case, NO concentration is determined from photons emitted by reaction with a high-concentration ozone reagent gas produced by UV irradiation of oxygen. The measurement is calibrated with a compressed NO standard of known concentration. The NO_2 concentration is determined by converting NO_2 to NO with a catalytic converter. The sum of NO and NO_2 is NO_x.

The NO_y inlet (*noy_bow_inlet*) is an addition to the NO/NO_2 analyser which converts other odd-nitrogen species such as nitric acid and peroxyacetylnitrate to NO. This converter is located at the air inlet on the bow crane. The measurement cycle for all the nitrogen species (NO, NO_2, NO_y) is controlled by the data acquisition system on the NO_x analyser. Data files for the NO_y inlet contain flag variables indicating the state of various valves that determine what is being measured at any particular time. Final computation of the concentrations for the various nitrogen species will be done post-cruise.

The slow ozone (*ozone_slow_ship_bow*) and gaseous elemental mercury (*hg_ship_bow*) analysers are both commercial instruments (TEI model 49C and Tekran 2537B).

The Gas Chromatograph–Mass Spectrometer (GCMS) system for volatile organics (*gcms_ship_bow*) is the combination of a custom-built sample collection/standardization system and a commercial GCMS (Agilent 7820A GC / 5977B MSD). Table 3.5.3 lists the target compounds for this analysis. Calibration is with compressed gas standards from NOAA and UEA. Computation of gas concentrations requires proprietary software from Agilent and will only be done post-cruise.

The dynamic flux chambers (*co2_ch4_chamber_portable*, *dms_chamber_portable*) are custom-built for flux measurements directly on snow, ice or water surfaces with a small footprint (<1m^2) and over short temporal scales of <1hr (e.g. Gao et al, 2011). A constant flow of ambient air (8 LPM) is maintained through the chamber volume. Concentrations of CO_2 and CH_4 are measured in the air entering and exiting the chamber using commercial, portable cavity-enhanced greenhouse gas analysers (Licor models 7810 and 7815). The surface flux estimate is derived from the differential concentration of air entering and exiting, the flow rate through the chamber, and the chamber footprint area. DMS concentrations entering and exiting the chamber are determined by gas chromatographic analysis of adsorbent traps. The

DMS adsorbent trap system operates in parallel to the CO_2/CH_4 analysers. Valves controlling the sampling of inlet and outlet air are programmed with a datalogger (Campbell Scientific model CR6), which also records the chamber flow rate and temperature.

In addition to the air measurements, open lead and melt pond water samples were collected in coordination with chamber flux deployments and analysed for DMS in our container lab on E deck.

Preliminary (expected) results

Dynamic flux chamber measurements were used to determine exchange of CO_2, CH_4 and DMS over the varied surfaces. These measurements aimed to investigate the relative contributions of the different ice/snow, melt pond and open lead surfaces to total CO_2, CH_4 and DMS exchange. CO_2 and CH_4 exchange rates were measured over 54 individual deployments of the dynamic chamber system over 24 days on both snow/ice and water surfaces. DMS exchange rates were measured during 50 deployments of the combined system. The total amounted to 18 measurements over ice/snow; 9 on melt ponds; and 23 on open leads (Table 3.5.2). We also performed 4 blanks. Preliminary CO_2 data suggest a relatively small negative flux (<-1 mmol/m^2/day on average) on ice and melt ponds, and below detection limit fluxes on snow (Figure 3.5.2). CO_2 fluxes on open leads were more pronounced and varied with mixing conditions (fresh water lens, wind speed). Open lead and melt pond flux measurements were combined with characterisation of the DMS, pCO2, and salinity profiles to investigate the impact of the freshwater lens on gas exchange (see chapter on cross-cutting activities and Table 3.5.4 for the list of device operation IDs). Snow/ice flux measurements were combined with microCT analysis to investigate the impact of snow/ice structure on gas exchange. We also deployed our dynamic flux chamber next to D. Nomura's closed chamber for intercomparison. Preliminary CO_2 data suggest a relatively good agreement between the two systems (Figure 3.5.3).

Turbulent flux measurements from the ship bow tower operated for most of Leg 5 (Fig 3.5.1), but the 10-min mean relative wind direction was within the desired +/- 60° sector only 26% of the time (Figure 3.5.4). The relative wind direction was within a +/- 120° sector about 70% of the time, so bulk gas concentration measurements are uncontaminated for most of this leg. Southerly winds predominate during Leg 5 (Figure 3.5.5) and easterlies are next-most-common. Northerly and westerly winds were least frequent. We therefore expect trace gas data to show significant influence from continental and marine sources during Leg 5. Nevertheless, DMS concentrations were variable and generally decreasing over the course of the leg, with quite low concentrations after the onset of freezing, even during the exit transit in the marginal ice zone (Figure 3.5.6).

Measurements at the Met City site were quite successful during leg 5 due to the favourable location south of the ship in a clean wind sector, sampling air over a mixed surface of open leads, ridges and remnant first-year ice. CO_2 and CH_4 fluxes measured at Met City were close to the eddy correlation detection limit, but show a slight tendency for negative flux at the start of the leg, decreasing to near zero as freezing progresses. More analysis is necessary to refine the flux estimates further.

Data management

All data are handled, documented, archived and published following the MOSAiC data policy (see APPENDIX). Raw data for all sensors has been archived on MCS. Discrete sampling events have been registered in the DShip ActionLog. Some of these discrete samples (air flasks and water samples for iodide) will be analyzed post-cruise and data are not immediately available. We are not directly involved in the analysis of these samples and cannot estimate a completion date at this time.

Data will be stored at the Arctic Data Centre following the agreement between ADC and the MOSAiC Project lead. DOIs will be communicated to PANGAEA for later access via the future MOSAiC Data Portal.

References

Bariteau, L, D Helmig, CW Fairall, JE Hare, J Hueber and EK Lang, (2010), Determination of oceanic ozone deposition by ship-borne eddy covariance flux measurements, *Atmos Meas Tech*, **3**, 441–455, doi:10.5194/amt-3-441-2010

Blomquist, BW, BJ Huebert, CW Fairall, and IC Faloona (2010), Determining the air-sea flux of dimethylsulfide by eddy correlation using mass spectroscopy, *Atmos Meas Tech*, **3**, 1–20, doi:10.5194/amt-3-1-2010

Gao, and others (2011), Chapter 9: Vapor flux measurements–Chamber methods, in: *Vapor Emission to Outdoor Air and Enclosed Spaces for Human Health Risk Assessment: Site Characterization, Monitoring and Modeling,* Nova Science Publishers, Hauppauge, NY, pp. 191-207.

FIGURE / TABLE CAPTIONS

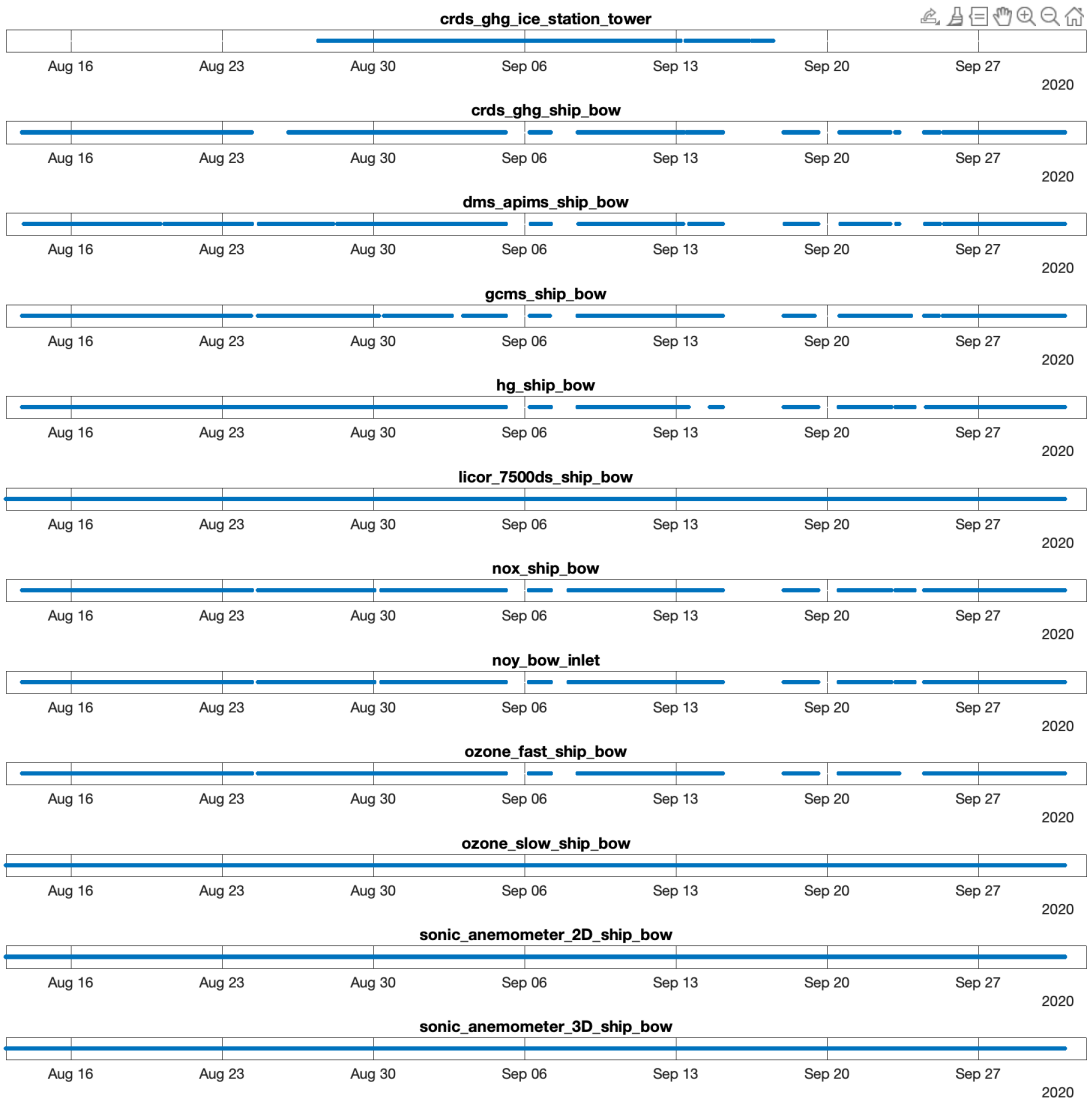

Figure 3.5.1: Operational timelines for continuous measurement systems deployed during Leg 5.

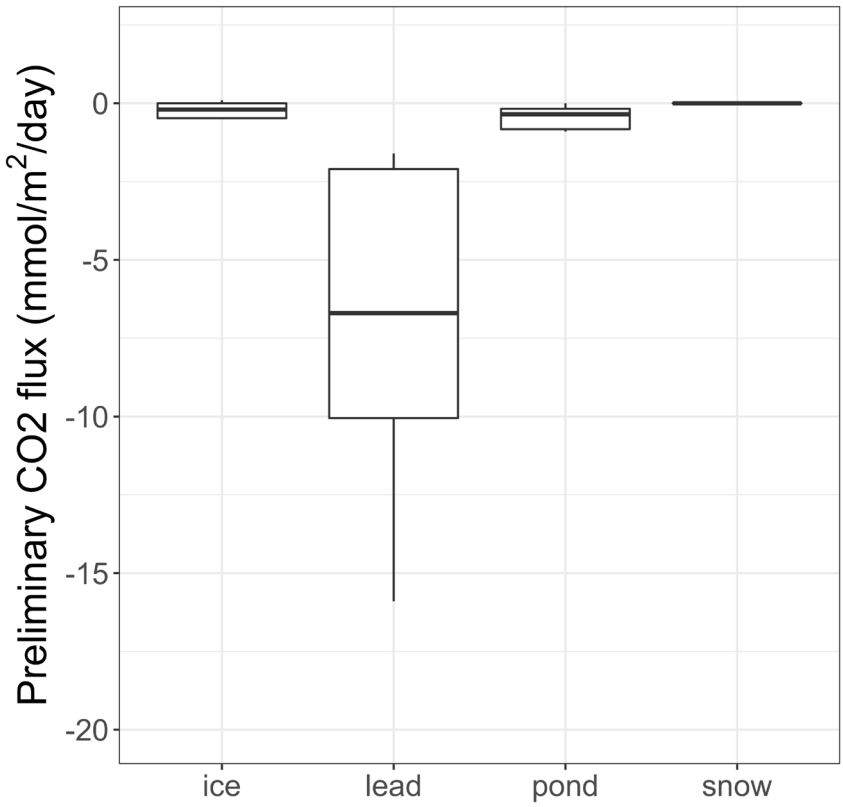

Figure 3.5.2: Preliminary CO_2 fluxes with the dynamic chamber surface flux system during Leg 5.

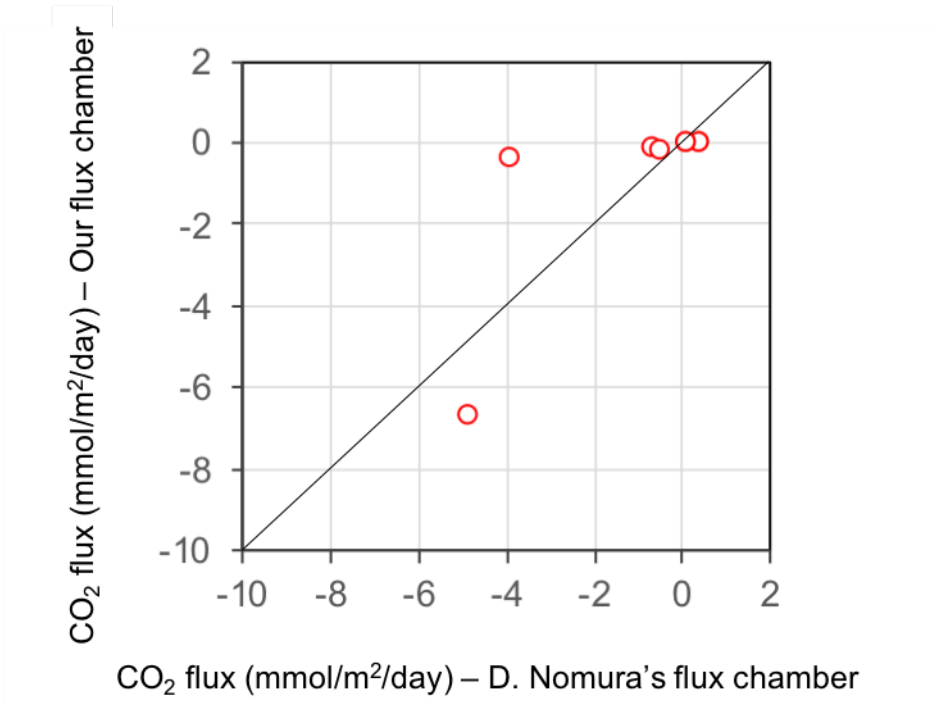

Figure 3.5.3: Intercomparison of the CO_2 flux chambers during Leg 5. The black line is the bisector.

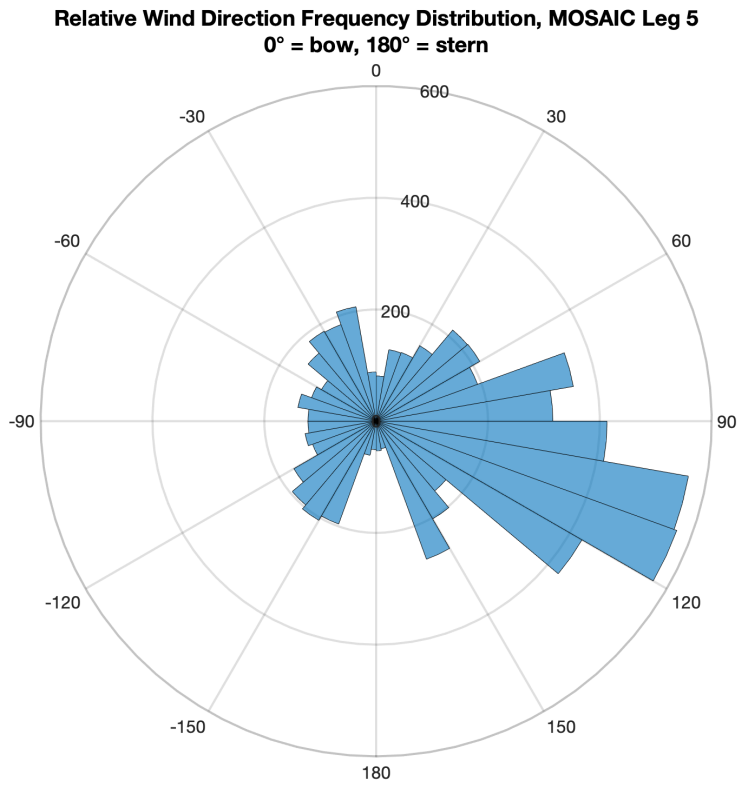

Figure 3.5.4: Polar frequency distribution histogram of 10-minute mean relative wind direction at the ship bow tower.

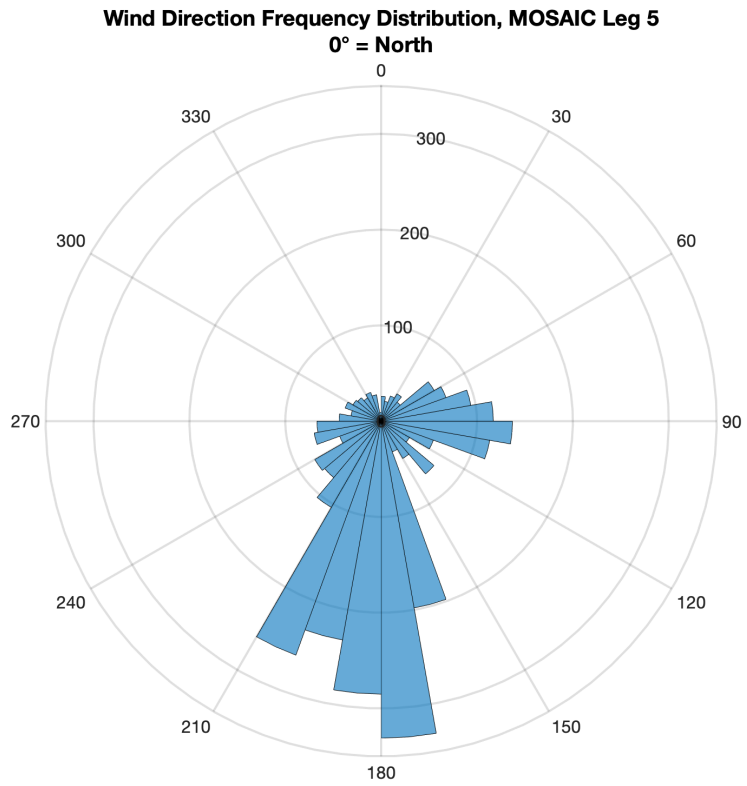

Figure 3.5.5: Polar frequency distribution histogram of 10-minute mean true wind direction.

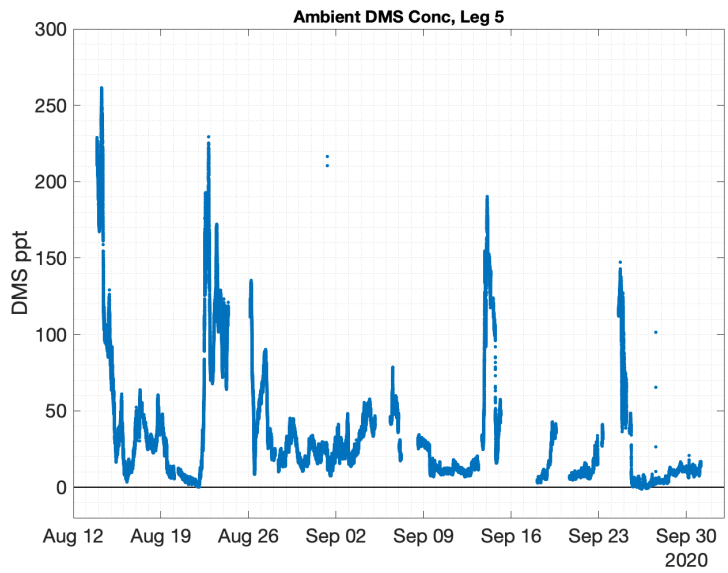

Figure 3.5.6: Atmospheric DMS concentration (ppt) during Leg 5 as measured by *dms_apims_ship_bow*.

Table 3.6.1: Trace Gas Flux/Reactive Gases Group, Instruments on MOSAiC Leg 4

Measurement System	Sampling Location	Sample Rate	SensorWeb 'Short Name'
DMS API Mass Spectrometer	ship bow tower	10 Hz continuous	dms_apims_ship_bow
Picarro G2311-f CRDS	ship bow tower	10 Hz continuous	crds_ghg_ship_bow
Chemiluminescent Ozone	ship bow tower	10 Hz continuous	ozone_fast_ship_bow
Metek uSonic-3 Anemometer	ship bow tower	10 Hz continuous	sonic_anemometer_3D_ship_bow
Licor 7500DS	ship bow tower	10 Hz continuous	licor_7500ds_ship_bow
RM Young 86004 Anemometer	ship bow tower	1 Hz continuous	sonic_anemometer_2D_ship_bow
Chemiluminescent NO/NO2	ship bow crane	10 per minute	nox_ship_bow
NOy inlet for NO/NO2 Analyzer	ship bow crane	10 per minute	noy_bow_inlet
TEI model 49C ozone analyzer	ship bow crane	1 per minute	ozone_slow_ship_bow
Tekran 2537B mercury analyzer	ship bow crane	1 per 5-15 minute	hg_ship_bow
Agilent GC Mass Spectrometer	ship bow crane	~15-18 per day	gcms_ship_bow
Picarro G2311-f CRDS	met city 10m tower	10 Hz continuous	crds_ghg_ice_station_tower
CO2/CH4 Flux Chamber	various	1-3 per deployment	co2_ch4_chamber_portable
DMS Flux Chamber	various	1-3 per deployment	dms_chamber_portable
Ozonesonde Profiler	tethered balloon	1 Hz continuous	ozone_profiler
Geenhouse Gas Flask Sampler	various	~ weekly	gmd_flask_sampler
VOC Flask Sampler	various	~ weekly	uea_flask_sampler

Table 3.5.1: Instruments deployed during Leg 5.

Table 3.6.2. Flux Chamber Deployments, MOSAiC Leg 5

Deployment Date	Number of Measurements				Gas Species		
DD/MM/YY	ice/snow	pond	lead	blank	CO2	CH4	DMS
22/08/20	1	1			X	X	X
25/08/20	1	1	1		X	X	X
26/08/20	1		2		X	X	X
27/08/20			2	1	X	X	X
28/08/20	1	2			X	X	X
29/08/20			2		X	X	X
31/08/20	1	1			X	X	X
01/09/20		2	1		X	X	X
02/09/20		2		1	X	X	X
04/09/20			1		X	X	X
05/09/20			2		X	X	X
07/09/20			3		X	X	X
08/09/20	1		1		X	X	X
09/09/20	1		1		X	X	X
10/09/20	2			1	X	X	
11/09/20	2				X	X	X
12/09/20	2			1	X	X	X
13/09/20	1				X	X	
14/09/20			1		X	X	X
15/09/20			2		X	X	X
17/09/20			2		X	X	X
24/09/20	2				X	X	X
26/09/20	1		1		X	X	X
30/09/20	1		1		X	X	X
TOTALS	***18***	***9***	***23***	***4***			
TOTAL	**54**						

Table 3.5.2: Deployments of the dynamic chamber surface flux system during Leg 5.

Table 3.6.3: Target Compounds for GCMS Analysis

Hydrocarbons	Halogenated Compounds	Other
Ethane	HFC-125	SF_6
Propane	HFC-134a	OCS
Propyne	HFC-152a	CS_2
Acetaldehyde	HFC-22	Dimethylsulfide
iso-Butane	Methyl Chloride	
n-Butane	CFC-12	
Acetone	HCFC-142b	
iso-Pentane	Methyl Bromide	
Isoprene	HCFC-124	
n-Pentane	H-1211	
Benzene	CFC-114	
Toluene	CH_2Cl_2	
	Methyl Iodide	
	HCFC-141b	
	CFC-11	
	CFC-113	
	chloroform	
	CH_2BrCl	
	CH_2Br_2	
	CCl_4	
	Perchloroethylene	
	$CHBrCL_2$	
	$CHBr_3$	

Table 3.5.3: Target compounds for GCMS measurements during Leg 5.

Table 3.6.4.: Flux Chamber Deployments - Device operation ID, MOSAiC Leg 5			
Deployment Date	Location name	Gas Species	
DD/MM/YY		CO2 and CH4	DMS
LEAD			
25/08/20	RS Lead	PS122/5_59-448	PS122/5_59-451
26/08/20	Met City Lead	PS122/5_59-455	PS122/5_59-456
	Met City Lead	PS122/5_59-459	PS122/5_59-460
27/08/20	Met City Lead	PS122/5_59_463	PS122/5_59_464
	Met City Lead	PS122/5_59_465	PS122/5_59_466
29/08/20	OC Lead	PS122/5_59_473	PS122/5_59_474
	RS Lead	PS122/5_59_475	PS122/5_59_476
01/09/20	RS Lead	PS122/5_60-187	PS122/5_60-188
04/09/20	ROV Lead	PS122/5_60-195	PS122/5_60-196
05/09/20	ROV Lead	PS122/5_60-197	PS122/5_60-198
	ROV Lead	PS122/5_60-199	PS122/5_60-200
07/09/20	OC Lead	PS122/5_61-16	PS122/5_61-17
	OC Lead	PS122/5_61-18	PS122/5_61-19
	OC Lead	PS122/5_61-20	PS122/5_61-21
08/09/20	OC Lead	PS122/5_61-39	PS122/5_61-40
09/09/20	OC Lead	PS122/5_61-118	PS122/5_61-119
14/09/20	Ship Lead	PS122/5_62-76	PS122/5_62-77
15/09/20	Ship Lead	PS122/5_62-78	PS122/5_62-79
	Ship Lead	PS122/5_62-80	PS122/5_62-81
17/09/20	Ship Lead	PS122/5_62-272	PS122/5_62-273
	Ship Lead	PS122/5_62-274	PS122/5_62-275
26/09/20	Ice Station 2	PS122/5_63-271	PS122/5_63-272
30/09/20	Ice Station 3	PS122/5_63-275	PS122/5_63-276
MELT POND			
22/08/20	Melt Pond by MetCity	PS122/5_59-364	PS122/5_59-365
25/08/20	Melt Pond by MetCity	PS122/5_59-450	PS122/5_59-452
28/08/20	MP4a	PS122/5_59_469	PS122/5_59_470
	MP4a	PS122/5_59_471	PS122/5_59_472
31/08/20	Coring	PS122/5_60-181	PS122/5_60-182
01/09/20	St3	PS122/5_60-183	PS122/5_60-184
	MP4a	PS122/5_60-185	PS122/5_60-186
02/09/20	MP4a	PS122/5_60-191	PS122/5_60-192
	MP4a	PS122/5_60-193	PS122/5_60-194
SNOW/ICE			
22/08/20	Melt Pond by MetCity	PS122/5_59-366	PS122/5_59-367
25/08/20	Melt Pond by MetCity	PS122/5_59-453	PS122/5_59-454
26/08/20	Met City Lead	PS122/5_59-457	PS122/5_59-458
28/08/20	MP4a	PS122/5_59_467	PS122/5_59_468
31/08/20	Coring	PS122/5_60-179	PS122/5_60-180
8/9/20	OC Lead	PS122/5_61-41	PS122/5_61-42
9/9/20	Snow Line by Balloon Town	PS122/5_61-116	PS122/5_61-117
10/9/20	Met City	PS122/5_61-149	no sample
	OC Lead	PS122/5_61-153	no sample
11/9/20	Snow Line by Balloon Town	PS122/5_61-171	PS122/5_61-172
	OC Lead	PS122/5_61-173	PS122/5_61-174
12/9/20	Met City	PS122/5_61-265	PS122/5_61-266
	Melt Pond by MetCity	PS122/5_61-267	PS122/5_61-268
13/09/20	Met City	PS122/5_61-269	no sample
24/09/20	Ice Station 1	PS122/5_63-267	PS122/5_63-268
	Ice Station 1	PS122/5_63-269	PS122/5_63-270
26/09/20	Ice Station 2	PS122/5_63-273	PS122/5_63-274
30/09/20	Ice Station 3	PS122/5_63-277	PS122/5_63-278

Table 3.5.4: Deployments of the dynamic flux system – List of device operation IDs.

3.6 MEASUREMENT-BASED UNDERSTANDING OF THE NEW PARTICLE FORMATION, AEROSOL BUDGET AND THEIR CLIMATE EFFECTS IN THE ARCTIC

Tiia Laurila[1] [1]FI.UNI-Helsinki

(not on board) Ivo Beck[2], Lauriane Quéléver[2], Tuija Jokinen[1], Julia Schmale[2], Mikko Sipilä[1], Tuukka Petäjä[1], Markku Kulmala[1] [2]CH.EPFL

Objectives

Low-level clouds have an important effect on the surface energy budget in the Arctic. Their lifecycles, warming and cooling effects over the central Arctic Ocean remain unclear, and models fail to correctly simulate them. This shortcoming is partly due to insufficient information on cloud phase (liquid and/or ice crystals). Particularly liquid droplets modulate cloud radiative properties responsible for warming[6]. Droplets form on cloud condensation nuclei (CCN), a subset of aerosol particles. Aerosol particle concentrations over the central Arctic Ocean can be extremely low such that cloud properties are strongly influenced by CCN availability, and in extreme cases cloud formation is even inhibited. Information on aerosol is scarce for all seasons in the high Arctic, but in particular for the cold and dark period when clouds have a pronounced warming effect. To date, only information from land-based stations further south provide proxy information on central Arctic Ocean aerosols in winter.

Our guiding research questions are as follows:

- What are the contributions of natural versus anthropogenic sources to central Arctic Ocean CCN concentrations and how do they vary throughout the seasons (e.g. full sea ice cover in winter vs marginal ice zone in summer)?
- How do new particles form in the Arctic and what is their chemical composition?
- What grows the newly formed particles larger in size?
- Are newly formed particles a source of CCN?
- Which key natural processes are likely to change the CCN budget and control cloud properties with global warming (e.g. diminishing sea ice)?
- How strongly are liquid cloud radiative properties controlled by availability of CCN throughout the seasons?
- What are natural sources of aerosol in general and CCN in particular during the polar night?

With our dataset, we will shed light on the contribution of anthropogenic emissions, other than greenhouse gases, to Arctic warming through cloud formation, characterize for the first time aerosol-cloud interactions during Arctic winter, and help evaluate and improve models for better predictions of Arctic climate change and its far-reaching consequences.

Work at sea

The UHEL-PSI team continued to collect a continuous data set during leg 5. Our in-situ measurements of aerosol physical and chemical properties, and aerosol precursor and air ion measurements are collected from two containers located on the C-deck on the bow area (position C10, EPFL-PSI container, and C9, BAS container). On top of running the PSI-UHEL instrumentation, our task was also to deploy Colorado State University's portable aerosol sampler on various locations on the ice. On leg 5 the portable aerosol sampler was deployed in the areas surrounding remote sensing (lead), met city and fiber town (meltponds).

We operate the instrumentation behind a total inlet (GAW standard) that captures particles and droplets, and an interstitial inlet, which captures only particles that are unable to form cloud

droplets. New particle formation events and aerosol precursor gas composition are measured from a specifically designed NPF inlet. The mass spectrometer in the C9 container measures from a simple stainless steel inlet mounted through the roof (APi-ToF inlet). See Figure 3.6.1 for an overview of inlets.

Real-time measurements are carried out by one person during each leg. The main tasks of the operator include ensuring high quality performance of the complex instrumentation set up and maintaining them during the leg. This person's responsibilities also included quality assurance of the measured data set and characterization of natural and anthropogenic events that influenced aerosol formation and population.

With a few exceptions, all instruments operated from the start of leg 5 until arrival to the 12 nautical mile zone around Svalbard. An overview of all instruments and their working periods is shown in Table 3.6.1. Smaller data gaps that lasted less than one day and are not listed.

Table 3.6.1: *Instrumentation and operating periods*

ID	Instrument	Location - Inlet	Application	Sampling period
CPC 3776	Condensation particle counter	C10 – Total	Aerosol concentration of the total particle population > 3 nm	12.8.2020 – 1.10.2020
CPC 3025	Condensation particle counter	C10 - Interstitial	Aerosol concentration of the interstitial particle population > 2.5 nm	12.8.2020 – 1.10.2020
SMPS	Scanning mobility particle counter	C10 – Interstitial & Total	Size spectrum of aerosol population between 14.0746 - 685.39 nm (period 1), and 10.366 – 486.97 nm (period 2)	12.8.2020 – 8.9.2020 15.9.2020 – 1.10.2020
PSM A11-1 in scanning more	Particle size magnifier	C10 - NPF	Size distribution of the smallest aerosol particles from 1 to 3 nm	12.8.2020 – 1.10.2020
PSM A11-2 in step mode	Particle size magnifier	C10 - NPF	Concentration of the smallest aerosol particles. 4 sizes between 1-3 nm.	12.8.2020 – 1.10.2020
NAIS	Neutral cluster and air ion spectrometer	C10 – NPF	Size distribution both neutral (2-42 nm) and naturally charged ions (0.8-42 nm). (electrical mobility equivalent diameter)	12.8.2020 – 1.10.2020
NAIS stern	Neutral cluster and air ion spectrometer	Stern – top of the cold storage container	Size distribution both neutral (2-42 nm) and naturally charged ions (0.8-42 nm). (electrical mobility equivalent diameter)	12.8.2020 – 1.10.2020
APS	Aerodynamic particle spectrometer	C10 - Total	Size distribution of the large aerosol population for aerodynamic diameters ranging from 0.5 to 20 µm	12.8.2020 – 1.10.2020
CCNC	Cloud condensation nuclei counter	C10 – Interstitial & Total	CCN concentration at supersaturations of 0.15, 0.2, 0.3, 0.5, 1.0 %	Not operational during leg 5.
WIBS	Wideband Integrated Bioaerosol sensor	C10 - Total	Measurement of fluorescently active aerosol for biological speciation between 0.8 and 20 µm	12.8.2020 – 1.10.2020

Aethalometer	Aethalometer	C10 – Interstitial & Total	Measurement of equivalent black carbon	12.8.2020 – 1.10.2020
AMS	Aerosol mass spectrometer	C10 – Interstitial & Total	Size-resolved chemical composition of submicron aerosol particles (e.g. sulfate, nitrate, organic, ammonium, chloride, …)	Not operational during leg 5.
CI-APi-TOF	Nitrate-based chemical ionization atmospheric pressure interface time of flight mass spectrometer	C10 - NPF	Aerosol precursor molecule composition measurements. (e.g. Sulfuric acid, Methane sulfonic acid, iodic acid, highly oxygenated organic compounds)	12.8.2020 – 1.10.2020
APi-TOF	atmospheric pressure interface time of flight mass spectrometer	C9 – roof inlet	Chemical composition of naturally charged anions and cations, (precursors of aerosols)	12.8.2020 – 1.10.2020
O_3	Ozone monitor	C10 - Interstitial	Ozone concentration	12.8.2020 – 1.10.2020
SO_2	SO_2 monitor	C10 - Interstitial	Sulfur dioxide concentration	12.8.2020 – 1.10.2020
SO_2	SO_2 monitor	C10 - Total	Sulfur dioxide concentration trace levels	12.8.2020 – 1.10.2020
Picarro	Picarro Analyzer	C10 - Interstitial	Gas-phase concentration of Methane, Carbon monoxide, Carbon dioxide, water vapor	12.8.2020 – 1.10.2020
RH / T 1 & 2	Temperature probe and hygrometer	C10 – Interstitial & Total	Relative Humidity and temperature sensor for both Interstitial and Total inlet	12.8.2020 – 1.10.2020
V1	Valve switch	C10 – Interstitial & Total	Hourly bases inlet sample switch for AMS, CCNC, Aethalometer, SMPS	12.8.2020 – 1.10.2020
CPC 3022	Condensation Particle counter	C10 - Interstitial	Aerosol concentration of the total particle population > 7 nm	12.8.2020 – 1.10.2020
C3PO	Optical particle counter and aerosol filter sampler	Various places across the central observatory	Coarse aerosol size distribution, filter sampling for ice nucleating particle concentrations	4 successful deployments on the ice floe

Expected and preliminary results

The difference between this and the previous legs is that leg 5 started in the open water meeting with the Akademik Tryoshnikov. The beginning of leg 5 included travelling into the ice in order to find a new ice floe. After leaving the ice floe on the 20th of September, Polarstern sailed along the ice edge in the marginal ice zone and crossed the ice edge multiple times. For atmospheric research, these were extremely important and valuable things to capture.

In the beginning of leg 5 efforst were made to recover the CCNC and the AMS. The turbo pump of the AMS was succesfully replaced and mechanically the instrument worked for the whole duration of leg5. However, the software was compromised and data acquisition could not be started again. The software was reverted back to earlier configurations, but unfortunately the problem could not be resolved. A pressure control board of the CCNC was also replaced, but

it did not resolve the issue. Further attempts to calibrate the flows and to diagnose the issue were made during the leg, but the reason for the problem could not be identified. The CPC of the SMPS malfunctioned during leg 5. This malfunction was seen as a high background during zero measurements. The optical unit of the CPC was opened for visual examination and cleaning, but after several attempts it seemed that the problem was something more complicated which could not be fixed during the expedition. The CPC was replaced with a spare CPC (TSI 3022). Using the spare CPC the SMPS could no longer sample from the valve and it was rerouted to sample from the total inlet.

During leg 5 we detected a few beautiful NPF events, for example on 25.8.2020 (Figure 3.6.2). The new particle formation can also be seen in the comparison of the CPC and the ultrafine CPC measuring in paraller from the interstitial inlet (Figure 3.6.3).

If these freshly formed particles actually grew up to CCN sizes, has to be studied further. For this, we will collaborate with ARM aerosol laboratory since our CCN counter was broken during this leg. Also, collaboration with Beluga balloon aerosol measurements with TROPOS is expected to find out the dimensions of NPF, is it happening only at close to ground level or are we observing formation of new particles in the whole boundary layer?

One valuable addition to our data set is the seasonal variation of aerosol particles and their precursor gases. MOSAiC campaign has now lasted more than an entire year and we can observe seasonal trends in our data. For example, in halogen compound concentrations (IO_3, HBr) are below the detection limit of our instrumentation during most of the polar night, but the sun rise starts a series of chemical reactions that produce halogenated compounds in the air. We detected higher concentrations of these compounds during summer but after midsummer they already started to decrease again. A huge task of post processing and analysing the data still avaits us even though the expedition is coming to an end. It will be interesting to see in more detail the phenomenas that we have seen climpses of during the measurements on board.

Data Management

All data are handled, documented, archived and published following the MOSAiC data policy (see APPENDIX). All instruments are registered in DShip as continuously recording instruments. All raw data are stored on the MCS. Raw data analyses will happen at the institutions involved and intermediate data products will be stored on the servers of the University of Helsinki and École Polytechnique Fédérale the Lausanne. Final data will be stored at the PANGAEA data repository (World Data Center PANGAEA Data Publisher for Earth & Environmental Science www.pangaea.de).

Figures & Figure Captions:

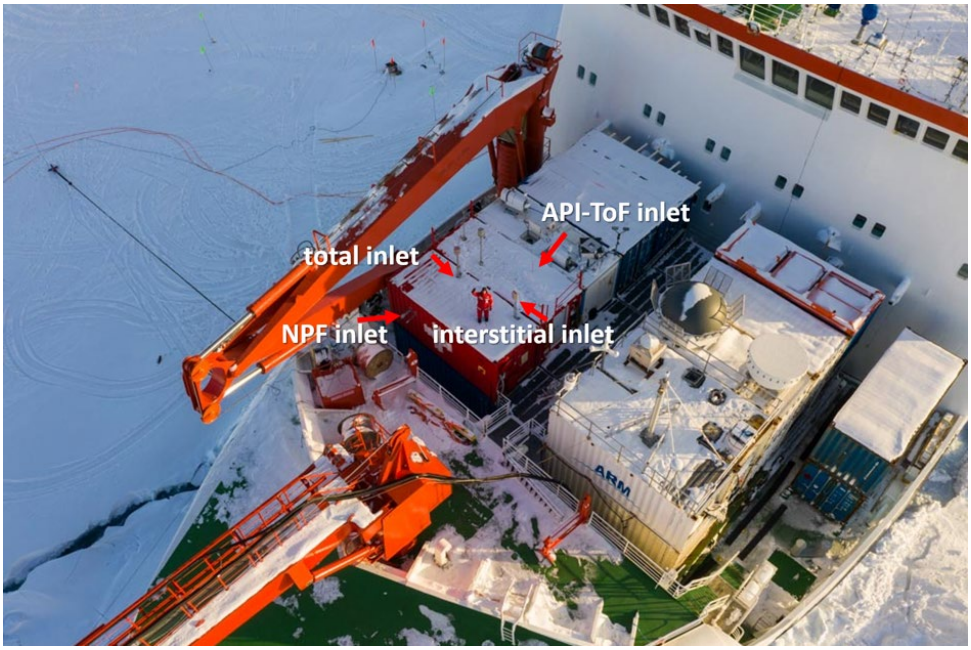

Figure 3.6.1: Inlets on the EPFL-PSI and BAS containers.

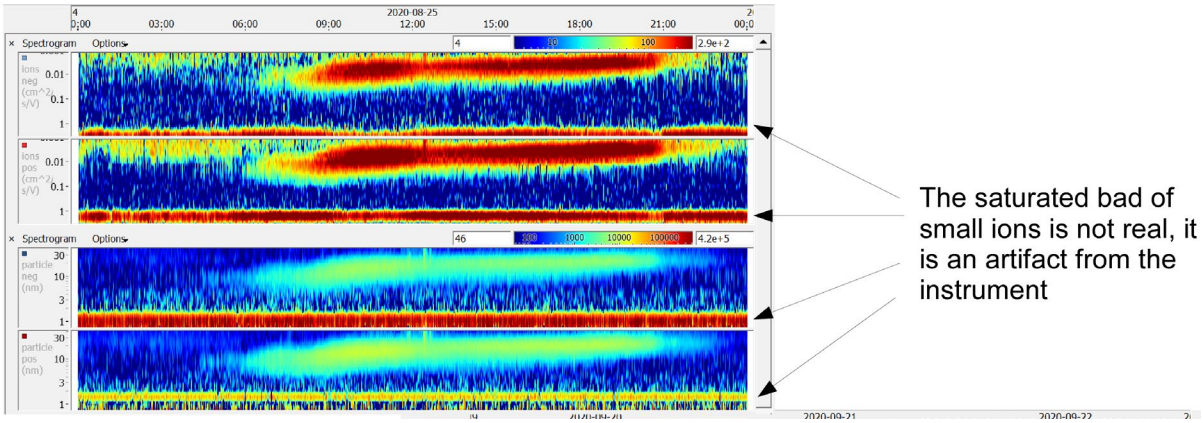

Figure 3.6.2: Screen shot of the neutral clusters and air ions (measured by a NAIS) during a new particle formation event. The two top panels represent anion and cations concentrations, while the two lower panel represent artificially charged neutral nanoparticles. Data artifacts appear at the bottom of each panel.

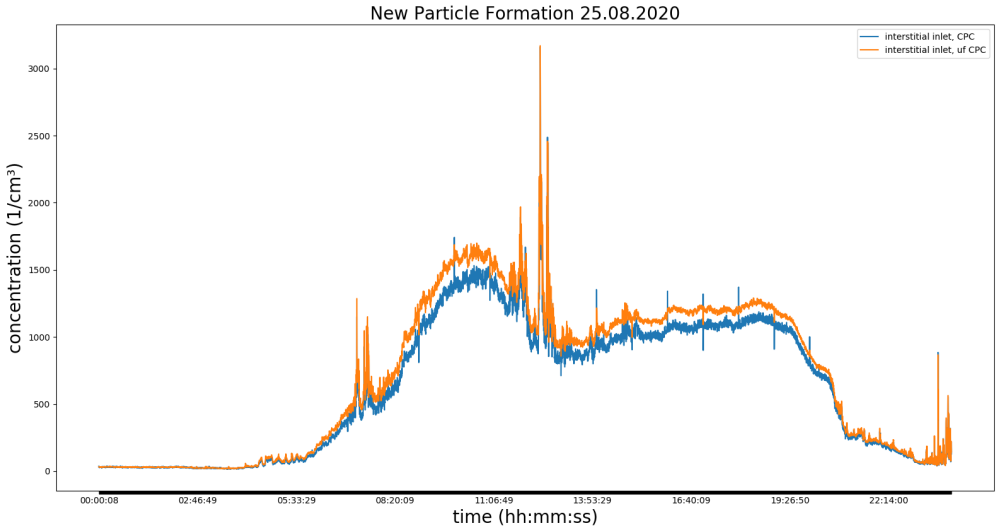

Figure 3.6.3: Comparison of CPC and ultrafine CPC measuring in parallel from the interstitial inlet. The NPF can be seen in the increase of the ultrafine concentrations as the new freshly formed particles are detected.

3.7 WIND AND TURBULENCE STRUCTURE IN THE ATMOSPHERIC BOUNDARY LAYER

Andreas Preußer[1] [1]DE.UNITRIER

(not on board), Ian Brooks[2], Ryan Neely III[2], Barbara Brooks[2], Günther Heinemann[1] [2]UK.UNI-LEEDS [3]EDU.CU [4]GOV.NOAA

Instruments attended by Dietrich Althausen[1] and Ola Persson[3,4]; text written by Ola Persson

Objectives

In order to better understand the new Arctic and its future development, improved numerical models and new verification data are needed particularly for the atmospheric boundary layer (ABL). The measurements will provide wind profiles with high spatial and temporal resolutions. In addition, Doppler wind lidar measurements allow for the determination of the turbulence structure of the ABL. A one-year long data set of wind and turbulence profiles will be generated for the verification of numerical models in the Arctic.

Overarching, the goal is to develop an enhanced understanding of the physical processes governing atmospheric boundary layer structure, turbulent mixing, and the interactions with both the surface and clouds in the central Arctic. This includes the following specific objectives:

- Characterize the turbulent dynamics of the Arctic atmospheric boundary layer and the physical processes controlling it over a full annual cycle. BL mixing directly affects the surface heat flux and both influences cloud properties and is influenced by in-cloud processes, and thus impacts the radiative fluxes and surface energy budget, contributing to ice formation/melt.
- Determine the interactions of Arctic boundary layer structure with the surface turbulent fluxes of momentum and heat. Surface fluxes are a controlling influence on lower BL structure. Elevated sources of turbulence, e.g. wind speed jets and radiative cooling at cloud top, dominate the control of upper BL structure and can impact surface fluxes where surface forcing of turbulence is weak, and thus the surface energy budget and ice evolution.
- Identify and describe the significant processes controlling coupling/decoupling of BL clouds to the surface. Decoupling isolates BL cloud from surface sources of moisture and aerosol; this may affect cloud properties (iii) and thus the surface radiation budget.

Work at sea

The boundary-layer dynamics measurements were obtained via active remote sensing instruments, which included three slightly different Doppler lidars and a phased array Doppler sodar. The University of Trier group supplied a Halo-Photonics Streamline (HPS) scanning wind lidar, which operates at a wavelength of 1.5 µm and is eye-safe. It was installed on board *Polarstern* on the lower P-deck in September 2019, alongside with a Galion G4000 wind-profiling lidar from the University of Leeds group. A nearly identical second HPS model was additionally provided by the Leeds group for operation on the pack ice along with their Scintec MFAS Sodar (Figure 3.7.2). However, the ULeeds lidar was brought on board at the end of Leg 3, and was moved to a new location on the port side of the Polarstern P-deck on Aug 18, 2020 for scanning during Leg 5 (Fig. 3.7.1). A new RHI scan program was installed on Sep 6, 2020, to complement that run by the University of Trier lidar on the starboard side.

The measurement-principle of the lidars relies on reflected light from particles in the atmosphere (aerosols, cloud droplets, and ice crystals). While the Halo lidars provide measurements of backscatter intensity and along-beam Doppler velocity, the Galion lidar solely provides Doppler velocity as an output. The two Halo lidars can in theory operate with a

maximum range of up to 10 km. However, previous campaigns have shown that the range is restricted by the low aerosol concentration in the Arctic and Antarctic, which can partly be compensated by increasing the averaging interval and adjusting the beam focus in order to optimize the signal-to-noise ratio (SNR), as recommended by Hirsikko et al. (2014). All used lidars are programmable scanning devices, which enable vertical scans in all hemispheric directions.

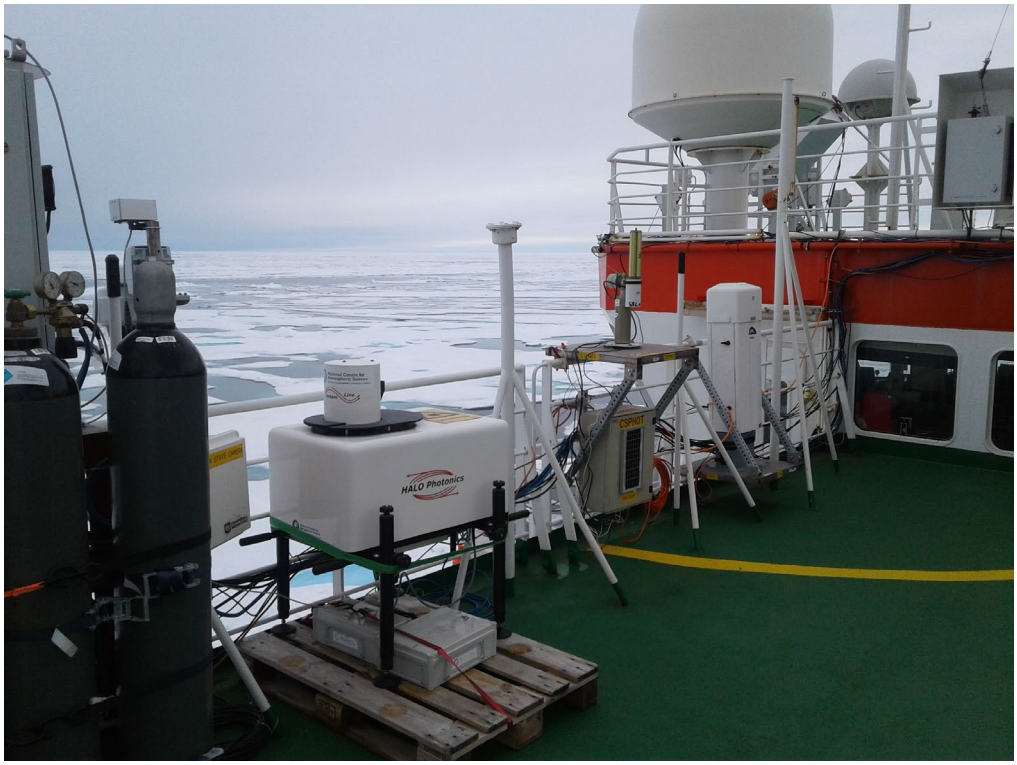

Fig. 3.7.1*: New location as of Aug 18, 2020, of the ULeeds HALO lidar on the port side railing of the P-deck (Photo: Ola Persson).*

For the Halo lidars, the main scan patterns that were used since Leg 1 include the range-height indicator (RHI), the vertical azimuth display (VAD) and vertical stares. RHI scans were performed with different elevation angles up to 50°. This allows for measurements of cross-sections, but also for vertical profiles of horizontal wind variances (TKE estimation, Banta et al. 2006). Vertical STARE data can be used to compute the vertical wind variance profile (see Päschke et al., 2015). The VAD scans are used for the determination of wind profiles above the lidar with multiple evenly spaced scans at an elevation-angle of 75° (e.g., Zentek et al., 2018). As for the Galion lidar, VAD scans with elevation-angles of 30° and 50° are continuously performed since the start of Leg 1.

For most of Leg 1 and 2 as well as the start of Leg 3, the Halo lidars were configured to operate independent from each other following the above described scan modes. However, despite the quite dynamic ice situation on Leg 3 it was again possible in late April to configure them to a synchronized mode, in which measurements of the same volume of air from two different directions ('virtual-tower') could be performed for 12 days in total. Unfortunately, frequent movement of the ice during Leg 3 made it difficult to initialize fixed scan parameters for the synchronized scans. During Leg 4, both Halo lidars were operated on the Polarstern P-deck. For Leg 5, the ULeeds Halo lidar was moved to the port side railing on the P-deck to complement the UTrier starboard side location. A partial RHI scan program was then started on the ULeeds lidar on Sep 6 in order that the two Halo lidars could obtain turbulence profile measurements in as many wind conditions as possible.

Fig. 3.7.2*: New location of the Scintec MFAS sodar at Leg 5 Met City (enclosure to the right), near 88 N, 105 E at the time of installation on Aug 26. (Photo: Ola Persson).*

The sodar uses acoustic backscatter to make its measurement. A sequence of audible acoustic pulses is transmitted. Echoes are returned from density gradients in the atmosphere – these arise primarily at gradients in temperature, either large scale gradients such as temperature inversions, or small-scale gradients resulting from turbulence. The intensity of the acoustic backscatter provides some information on the turbulent and thermodynamic structure of the lower atmosphere. The Doppler shift of the echo provides a measurement of air motion. The acoustic beam can be steered off the vertical, allowing measurements of horizontal wind components to be made giving another measurement of the wind profile. The sodar vertical resolution is 10m, with a range from 40-1000m (though the upper limit is strongly dependent upon conditions and rarely reaches this absolute maximum). Wind profiles are obtained at 10-minute intervals and vertical backscatter profiles every 5 minutes. The Leeds sodar was installed at the Leg 5 *Met City* and operated continuously from Aug 26 to the deinstallation of the site on Sep 18.

Preliminary (expected) results

All three lidars ran well on board the ship during Leg 5. Good sodar signals were observed on the monitor, with data generally up to 300-400 m, and once observed to 900 m.

Data management

All data are handled, documented, archived and published following the MOSAiC data policy (see APPENDIX). Raw data is archived on the MOSAiC central Storage (MCS) system, on a RAID belonging to Leeds and two external hard-drives. All data will be made available through the central MOSAiC archive on the PANGAEA data repository (World Data Center PANGAEA Data Publisher for Earth & Environmental Science www.pangaea.de). Derived data products require post-cruise data processing and will be archived with PANGAEA as soon as they are available.

References

Banta, RM, Pichugina, YL, Brewer, WA. (2006) Turbulent Velocity-Variance Profiles in the Stable Boundary Layer Generated by a Nocturnal Low-Level Jet, Journal of the Atmospheric Sciences, 63, 2700-2719

Hirsikko A, O'Connor E, Komppula M, Korhonen K, Pfuller A, Giannakaki E, Wood CR, Bauer-Pfundstein M, Poikonen A, Karppinen T, Lonka H, Kurri M, Heinonen J, Moisseev D, Asmi E, Aaltonen V, Nordbo A, Rodriguez E, Lihavainen H, Laaksonen A, Lehtinen KEJ, Laurila T, Petäjä T, Kulmala M and Viisanen Y (2014) Observing wind, aerosol particles, clouds and precipitation: Finland's new ground-based remote-sensing network. Atmospheric Measurement Techniques, 7. pp. 1351-1375. ISSN 1867-8548 10.5194/amt-7-1351-2014.

Päschke E, Leinweber R, and Lehmann V (2015) An assessment of the performance of a 1.5 µm Doppler lidar for operational vertical wind profiling based on a 1-year trial, Atmospheric Measurement Techniques, 8, 2251-2266, https://doi.org/10.5194/amt-8-2251-2015.

Zentek R, Kohnemann S, and Heinemann G (2018) Analysis of the performance of a ship-borne scanning wind lidar in the Arctic and Antarctic. Atmospheric Measurement Techniques, 11, 5781-5795, https://doi.org/10.5194/amt-11-5781-2018.

3.8. TEAM ATMOSPHERE CONTRIBUTIONS TO UNIQUE LEG5 FLOE CROSS-CUTTING ACTIVITIES

Michael Gallagher[1,2], Alexander Schulz[3], Sandro Dahlke[3], Ola Persson[1,2], Byron Blomquist[1,2], Dietrich Althausen[4], Roberta Pirazzini[5], Markus Rex[3,6]

(not on board:) Matthew Shupe[1,2], David Costa[1,2], Thomas Ayers[2], Christopher Cox[2], Daniel Gottas[2], Jesse Leach[2], Jackson Osborne[1,2], Sergio Pezoa[2], Don Perovich[5], Timothy Stanton[6]

[1]EDU.CU
[2]GOV.NOAA
[3]DE.AWI
[4]DE.TROPOS
[5]FI.FMI
[6]DE.UNI-Potsdam
[7]EDU.DARTMOUTH
[8]EDU.NPS

Objectives:

To adapt to the unique nature of MOSAiC's fifth leg, team atmosphere contributed to several unique experiments at the new MOSAiC floe. Contributions were made to the leg 5 intensive observing periods (IOPs), and ad-hoc experiments were designed to best utilize the instrumentation available for on-ice observations. These experiments are shortly termed as Hinterland, Fibertown, Fibertown Pond, Stress Line, Team Ice drone flights, and Ice Station slow transects. This section 3.8 details the atmospheric perspective and contributions to this work. More thorough discussions of the cross-cutting aspects of the research for these experiments can be found in Chapter **8(?)**

Intensive Observing Periods (IOPs)

During the time on the leg 5 floe, there were two IOPs coordinated across the MOSAiC teams. The IOP time periods were chosen primarily because of the unique cyclonic conditions and atmospheric structure forecasted in the days leading up to the IOP. In order to better capture the vertical structure of the atmosphere during the passing of these relatively large and deep cyclones.

For these IOPs launches of balloon-based radiosondes during these periods was doubled, with sondes launched every three hours during the 36 hour IOP period. This higher frequency allows for improved linkages of the thermal/kinematic sonde measurements with the much higher frequency remote sensing measurements, such as clouds, precipitation, boundary-layer structure, and trace gas sampling. It also allows additional understanding of the interdisciplinary on-ice measurements by the other teams. Upper ocean and even ECO sampling was done at such a rapid rate during these IOPs, that, for the first time, there seems to be a possibility to correlate atmospheric, surface, upper-ocean and ecology time series.

The IOPs were chosen based on forecasts of atmospheric cyclones, where rapidly changing atmospheric conditions, including SEB, strong surface winds, and ice movements were all likely to produce rapid changes for the other disciplines. The two IOPs done were Sep 6-7 and Sep 13-15. These two periods included the strongest winds and lowest sea-level pressure during the floe drift (see Fig. 3.4.6); the wind forecasts for IOP1 were initially much stronger than were actually observed. The temperatures remained below freezing for IOP1 but some brief surface melt occurred during IOP2, especially during a rain-on-snow period that significantly changed the ice surface characteristics (see Fig. 3.4.5). The atmospheric enhanced soundings started earlier in IOP2 because of forecasts of precipitation beginning earlier than the strong winds, leading to a longer IOP. Preliminary analyses of quick-look KAZR

radar images overlaid on sounding time-height cross-sections and utilizing a variety of surface parameters demonstrate the key atmospheric features (e.g., low-level jets, frontal passages, precipitation phase transitions, lower troposphere temperatures, small-scale tropopause eddies) that impact the surface energy budget (including albedo), ice movement, trace gas concentrations, and even likely upper-ocean mixing. Figure 3.8.1 shows one of these analyses using the soundings and ship data.

The increased soundings during the IOPs captured well the structure and passage of these unique cyclones, even on the mesoscale. This was particularly important for IOP2, which was quite complex and demonstrated surprisingly rapid changes in the thermodynamic and kinematic structure not just at lower levels, but even near the tropopause. More details of the interdisciplinary impacts observed during these events are presented in **Chap. 8?.**

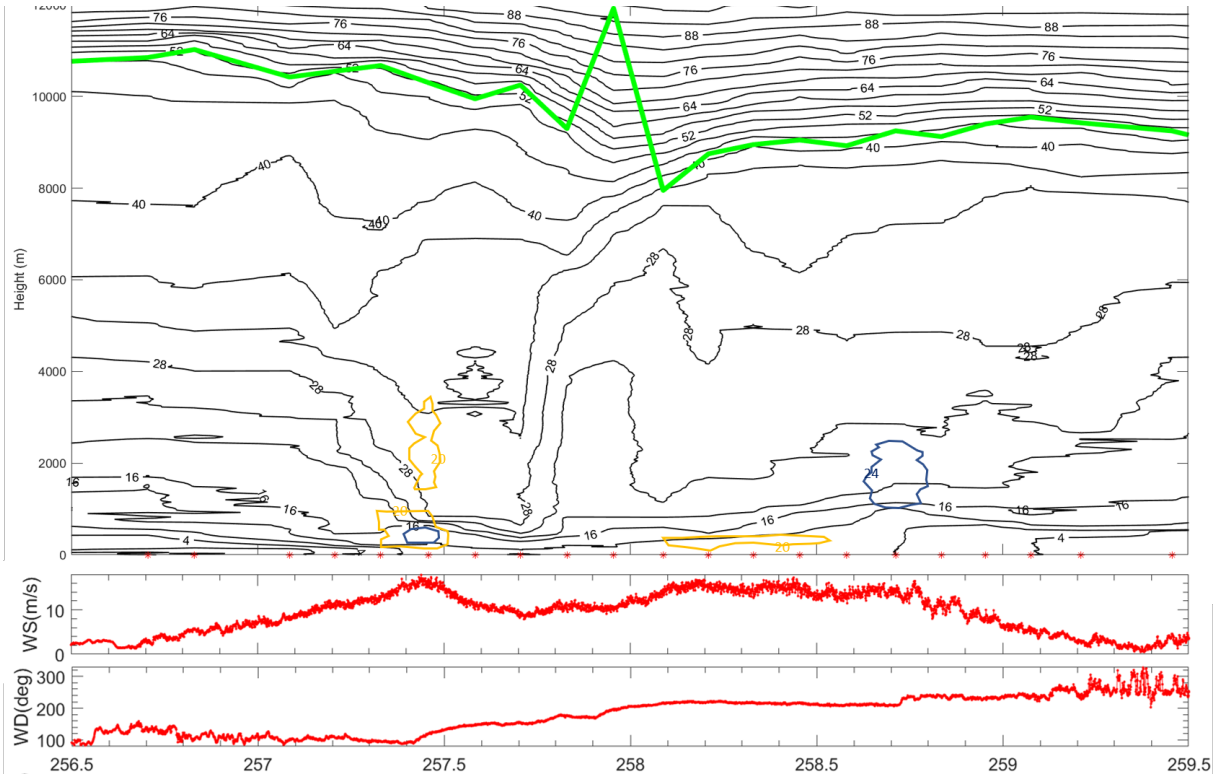

Fig. 3.8.1*: Time-height section of equivalent potential temperature (isopleths, deg C) from serial soundings during IOP2. The red stars at the surface indicate time of sonde launches, showing the 3-hourly interval. The green line represents the tropopause (defined as the local temperature minimum), and the yellow and blue isopleths represent select 20 m/s and 24 m/s isotachs, respectively, at locations of low-level jets. The red traces below show the wind speed and wind direction from the ship's instruments.*

Cross-cutting experiments on-ice

The Hinterland Experiment — studying the spatial heterogeneity of surface energy fluxes, including radiation and turbulence

As MOSAiC Leg 5 takes place after the demise of the original floe, there were opportunities to design new experiments on Leg 5 floe. For "the Hinterland Experiment", the ATMOS team coordinated with other MOSAiC teams to compliment observations of key atmospheric parameters with observations of snow structure, ice properties, and spatial albedo. For a broad overview and table of cross-cutting observations made for the Hinterland Experiment, see:

In the Hinterland, team ATMOS deployed one CU/NOAA ASFS flux station (ASFS30, see section 3.4), and two AWI Eddy Sledges (see section 3.1). The deployment of the AWI sledges in line with ASFS30 produced the “stress line” running from a ridge region to the flatter FYI. A visual image of the configuration of these instruments is shown in Fig 3.8.2

The ATMOS component of the Hinterland Experiment was designed with three primary considerations: 1) obtaining unique SEB observations with the large instrumentation suite from ASFS30 2) placing the 3 sledges in a configuration that generates valuable complimentary turbulence data 3) positioning the sledges well relative to the ship to obtain the best possible observations, ideally with a clean wind fetch from the port side of the ship to compliment observations made at Met City.

With these considerations, the Hinterland site was located to the aft of the Polarstern across a recently closed lead at the edge of the Leg 5 floe camp. ASFS30 was placed directly into an unfrozen melt pond to capture the SEB variability during melt pond refreezing, a unique observation for both MOSAiC and the central Arctic (see Fig 3.8.2). The presence of the pond impacts both the shortwave and longwave radiation, and possibly also the turbulent heat fluxes (Fig. 3.8.3). Hence, the SEB is greatly altered. With the large number of melt ponds on the drift floe, it is important to make the measurements of the SEB evolution over this surace.

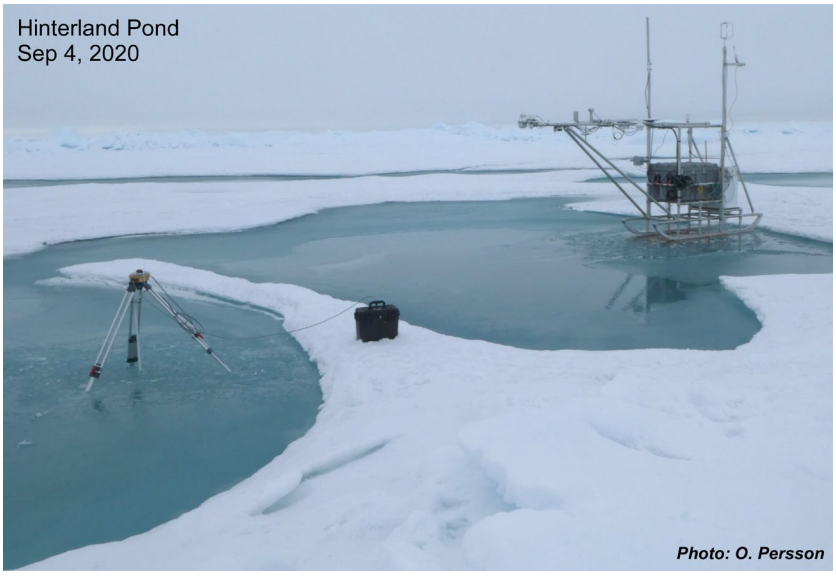

***Fig. 3.8.2**: Deployment of ASFS30 and a thermistor string (courtesy M. Hoppmann, Team Ice, AWI) at the Hinterland Pond on Sep 4, 2020.*

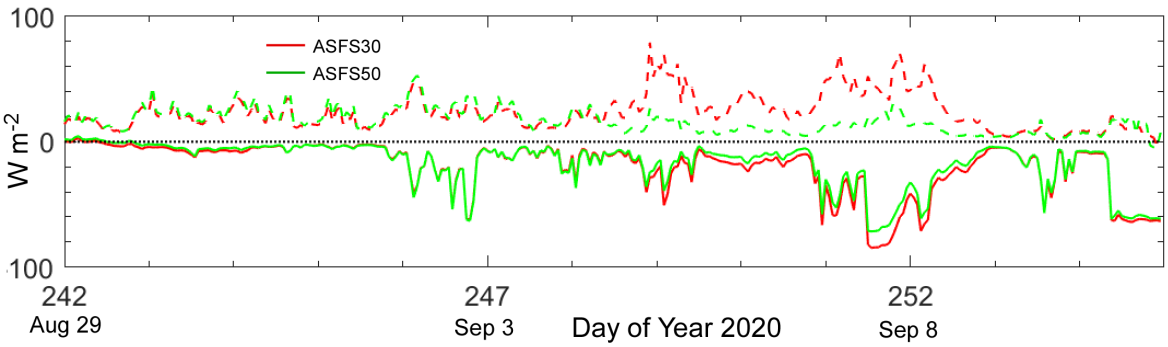

***Figure 3.8.3**: Preliminary net shortwave (dashed) and net longwave (solid) radiation at ASFS30 and ASFS50 from Aug 29 through Sep 10, 2020. ASFS30 was moved to Hinterland Pond on Sep 4, near 08 UTC.*

The ASFS30 melt pond was located roughly 50 meters from a tall and broad ridge running parallel to the orientation of ***Polarstern***. As such, the AWI eddy sledges were then placed perpendicular to the large ridge. One eddy sledge was located inside of the ridge nearer to the location of Polarstern and roughly 200m aft, approximately 70 meters from ASFS30. The second eddy sledge was located on the far side of ASFS30, away from the ridge, in a relatively homogeneous and flat region of ice.

Thus the following concepts may be investigated using observations made during the Hinterland experiment. The complete SEB variability of a melt pond during the refreezing period. The stress variability in different ice surface topography. The spatial heterogeneity of turbulent energy fluxes in varying ice surface topography. The impact of a ridge on the lee and windward turbulent structure of the surface layer during transverse flow.

These Hinterland Experiment data are available from approximately 12:00 UTC on September 4th until 0600 UTC on September 19th. The described scientific concepts can be investigated using the following atmospheric parameters measured by the three sledges:

Variable	Instruments	Installation Locations
Surface Conductive Heat Flux (at ice snow interface)	Hukseflux Flux plates	ASFS30 pond
P, T, RH – 2m	Vaisala PTU337	ASFS30 pond
Fast response winds – 2m	Metek Sonic anemometer	ASFS30 pond
Fast response winds – 2m	Licor Sonic anemometer	Eddy sledges
Fast water vapor and carbon dioxide – 2m	LICOR open path gas analyzer	ASFS30/Eddy sledges
Position and Heading, 2m	Hemisphere dual GPS	ASFS30/Eddy sledges
Surface height (snow depth, ice melt)	Campbell SR50 sonic ranger	ASFS30 pond
Infrared Surface Temperature	Apogee IRT	ASFS30 pond
Radiation: SW, LW, up and down, 2m	Hukseflux radiation suite	ASFS30 pond

As a final component of the Hinterland experiment, the three sledges were brought to a central and relatively smooth location to gather data for a cross-comparison of their sonic anemometers. The sleds were oriented perpendicular to forecasted winds such that they would not interfere with the comparison measurements. These data will be used to calibrate and better understand the turbulent flux observations made by the different instrumentation configurations in the Hinterland topographical regions. The intercomparison began near 12 UTC Feb 19, at the end of the Hinterland experiment, and continued overnight until they were

removed and returned to the ship for the departure of the **Polarstern** from the Leg 5 floe. Approximately 10 hours of useful data were obtained during this intercomparison.

Fibertown temperature profiling

OCEAN - Additional temperature profiling of the first 60m of the ocean below the ice with the distributed temperature sensing (DTS) system added to the 10m profile at Fiber Town.

In collaboration with the OCEAN team we put 60m of fibre cable into the ocean to continuously sample temperature variations of the upper ocean mixed layer at the same spot of the atmospheric temperature profiling. This installation was coordinated within the ATMO and OCEAN team to achieve an optimal sampling network and avoidance of inference with other ocean sensor deployments below the ice. The 60m continuous ocean temperature profiling of the ocean mixed layer complemented the discrete MSS and CTD profiles. In order to obtain the real physical depths of the drifting fibre cable below the ice we attached an additional pressure (and temperature) sensor (RBR Duet TD 85201 – DShip device operation: PS122-5_59-342, SensorWeb ID: 6785, contact: Mario Hoppmann, DE.AWI) to the lower end of the fibre optic cable.

Fibertown Pond radiation

ICE - Additional continuous measurement of the 4 radiation components over a freezing melt pond

In coordination with team ICE and team ATMO, the radiation sensor was installed at a melt pond next to the 10m mast with the Distributed Temperature Sensing (DTS) mast, so-called Fiber Town (see Figure 3.1.4). Fiber Town itself was located about 50m away from MetCity were radiation sensors targeted the snow/ice surface. This resulted in an optimized coverage of the local surface heterogeneity and the transition of the radiation budget (and albedo) during the freeze up could be sampled optimally. Several additional measurements within and on our melt pond had been done by the ICE team (contact: Felix Linhardt, DE.CAU) including spectrometer measurements (albedo), temperature and salinity profile (see list below). This had been done to achieve an optimal sampling of all relevant pond parameters.

Table 3.8.1 List of measurements done by the ICE team at our melt pond

DShip Device operation	Date	Device
PS122/5_59-482	2020-08-28	cau_stickle_1
PS122/5_59-355	2020-08-28	BUCKET_PS
PS122/5_60-273	2020-08-31	cau_boeoetle_1
PS122/5_61-311	2020-09-08	cau_stickle_1

ATMO Stress Line - form drag transect experiment

One of our planned process studies for MOSAiC was to characterize the impact of ridges on the local turbulence within the surface layer (EXPEDITION PROGRAMME PS122 Polarstern PS122 Tromsø – Bremerhaven 20 September 2019 – 14 October 2020, available via www.awi.de/en/reports). Due to the additional mobile eddy covariance (MEC) system on leg 5 (MEC2, DE.AWI), 2 eddy sledges had been available to construct a transect over a ridge with two identically equipped systems. During leg 3 a similar experiment had been conducted with one ASFS (Matthew Shupe, EDU.CU, GOV.NOAA) system and one MEC (Alexander Schulz, DE.AWI) in collaboration with the ATMO team (see Cruise Report leg 3). In leg 5 we coordinated a 3 sledges transect including both MEC systems and the ASFS30 sledge. MEC2

was positioned within the big ridge, ASFS30 on a freezing melt pond in about 130m distance out of the ridge and MEC1 in additional 130m distance away from ASFS30 on the flat area of the floe. This setup resulted in a transect of 3 eddy covariance systems with the following footprints (under optimal wind conditions): in ridge (turbulence dominated by ridge roughness), close to ridge (transition from ridge to flat ice), down ridge (flat ice). The transect experiment was running in the period from 5th to 18th September 2020.